Scientific Research Publishing

International Journal of Geosciences, 2022, 13, 199-243
https://www.scirp.org/journal/ijg
ISSN Online: 2156-8367
ISSN Print: 2156-8359

Geo-Hazard Susceptibility Assessment and Its Impacts on Livelihoods in Kerio Valley, Kenya

Mark Boitt[1*], John Gathoni[2]

[1]Institute of Geomatics, GIS and Remote Sensing, Dedan Kimathi University of Technology, Nyeri, Kenya
[2]Department of Research and Development, GIS and Remote Sensing Section-Mapinfotek, Nairobi, Kenya
Email: *mark.boitt@dkut.ac.ke, johnw@mapinfotek.co.ke

How to cite this paper: Boitt, M. and Gathoni, J. (2022) Geo-Hazard Susceptibility Assessment and Its Impacts on Livelihoods in Kerio Valley, Kenya. *International Journal of Geosciences*, **13**, 199-243.
https://doi.org/10.4236/ijg.2022.133011

Received: January 31, 2022
Accepted: March 19, 2022
Published: March 22, 2022

Abstract

Geohazards are a recurrent issue in the Kerio River catchment of Kenya, which usually results in life and property loss. This research focuses on mapping geo-hazard risk zones of the region. The risk zones were developed from a combination of land use land cover maps, agroecological zones maps and soil erosion maps using the Analytical Hierarchy Process method of multi-criteria analysis. The final results depict the geohazard risk maps which show the susceptibility of different areas in the catchment (classified as risk zones) to hazards. The zones range from no risk zones to very high-risk zones. The results showed that the lowlands are most susceptible to hazards as they were classified as high-risk zones. These risk zone areas have impacts on the socio-economic development hence negatively impacting livelihoods in the area.

Keywords

Kerio Valley Basin, Land Use Land Cover, Moisture Zones, Agroecological Zones, Soil Erosion, RUSLE Model, Geohazard Risk Zones, Multivariate Clustering, Analytical Hierarchy Process

1. Introduction

This research was done to determine the geohazard risk zones in the Kerio Valley of Kenya. Geohazard is derived from two words: geo meaning earth and hazard which refers to a situation that poses risk to the environment, property or life [1]. Risk involves determining how susceptible an area is to geohazards and their effects. Geohazards include but are not limited to earthquakes, floods, landslides, soil erosion, rock falls and volcanic eruptions. This study was done to establish geohazard risk zones as a product of multi criteria analysis of soil ero-

sion maps, agroecological zones maps and land use land cover maps.

Soil erosion is a form of land degradation that involves the removal the soil top layer by erosive agents such as wind, animals and rainfall. In the present study soil erosion was estimated using Revised Universal Soil Loss Equation (RUSLE) model, remote sensing data and GIS techniques in Kerio Valley. RUSLE model was developed as USLE to estimate soil erosion in croplands by Wischmeier and Smith in 1965. RUSLE is a computerized version of USLE with improvements in many of the factor estimates, which was initially released for public use in 1992 [2]. RUSLE model estimates soil loss as a product of five factors; rainfall and runoff erosivity, soil erodibility, slope length and steepness, cover management and conservation practice.

Agroecological zones (AEZ) are geographical areas exhibiting similar climatic conditions that determine their ability to support rainfed agriculture [3]. The zones range from the highly suitable for agriculture to those most unsuitable for rainfed agriculture. The zones are specific combinations of moisture availability zones and temperature zones [4].

Land use refers to the purpose land serves such as recreation areas while land cover refers to the surface cover on the ground whether vegetation, urban built-up or water [5]. Land use land cover maps were obtained from classification and analysis of satellite images for the years 1990 to 2020 at an epoch of ten years. This was done to show land use land cover changes in the basin over the given period of time.

Observed climate change is affecting agriculture through increased temperatures, changing precipitation patterns and greater frequency of extreme events occurring which directly affects food security [6]. Therefore, mapping of Kerio Valley agroecological zones is imperative to act as supportive mechanism of guiding the agricultural dynamics in the area of interest. The maps are necessary to support the local governments and residents in making data driven decisions as they need to address the increasingly sensitive food security issues.

Kerio valley is prone to increased occurrence of hazards especially flooding in the lowlands and landslides in highlands and escarpment due to immature geology, increased rainfall, rapid population growth and urban development [7]. This research was conducted to establish and map out the different risk zones and their susceptibility to occurrence of geohazards which is crucial for planning and development of warning systems by emergency evacuation organizations such as the Kenya Red Cross Society. The results from this study are vital in predicting where hazards are most likely to occur thus helping to warn residents and the local administrations of such incidences.

In this research multiple datasets were required to generate the geohazard risk maps. Multicriteria analysis techniques were required to evaluate the three different datasets, where Analytical Hierarchy Process (AHP) was chosen.

The objectives of this study were established as follows:

- To assess the land use land cover changes in the basin in 1990, 2000, 2010 and 2020,

- To determine the agroecological zones and assess the rate of potential soil loss in the basin in 1990 and 2020 respectively,
- To conduct a geohazard risk assessment to livelihoods of the basin.

2. Materials and Methods

2.1. Data

Table 1 below shows the different datasets and their sources that were collected and used to generate land use land cover maps, soil erosion maps and agroecological maps.

2.2. Software

Table 2 below shows all the tools and software that were used to process the datasets to produce the end results where each was used for specific purposes as outlined in the table.

2.3. Study Area

Kerio Valley Basin is located in the Rift Valley region of Kenya between the counties of Baringo, Elgeyo Marakwet and West Pokot as shown in Figure 1. River Kerio passes inside the basin and serves as the boundary between Baringo and Elgeyo-Marakwet counties.

2.4. Methodology

As shown in Figure 2 above temperature data was used to generate temperature

Table 1. Data.

Data	Source	Availability
Basin Boundary	World Resources Institute	Available
Satellite imagery	USGS Earth Explorer	Available
Temperature data	Terra Climate	Available
Rainfall data	CHIRPS	Available
Potential evaporation data	Terra Climate	Available
SRTM 30 m resolution DEM	RCMRD Geoportal	Available
Soil data	ISRIC DataHub	Available

Table 2. Software.

Software	Purpose
ENVI	Land use land cover mapping
ArcMap	AEZ mapping Geohazard risk assessment
QGIS	Soil erosion assessment using RUSLE

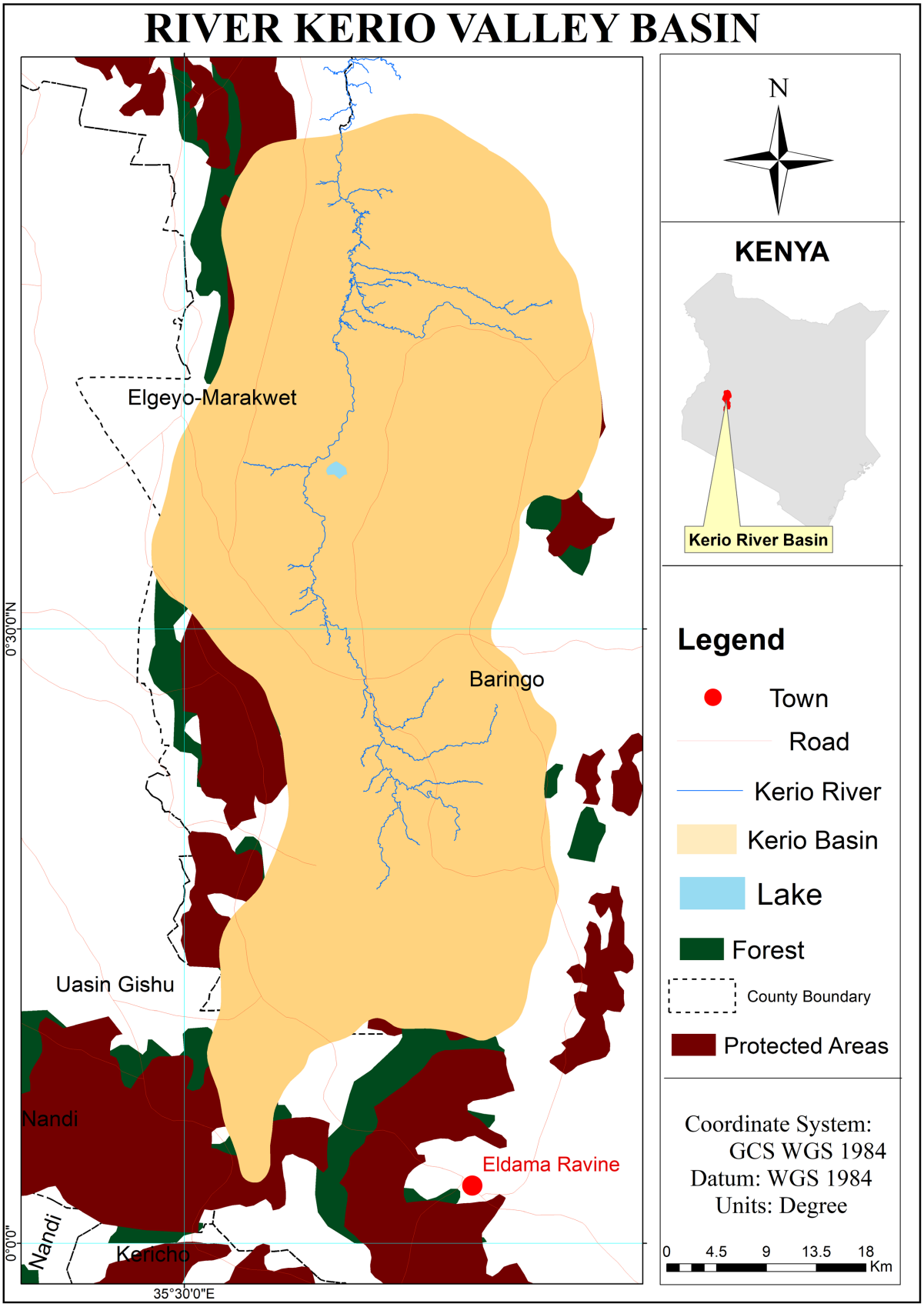

Figure 1. Study area map.

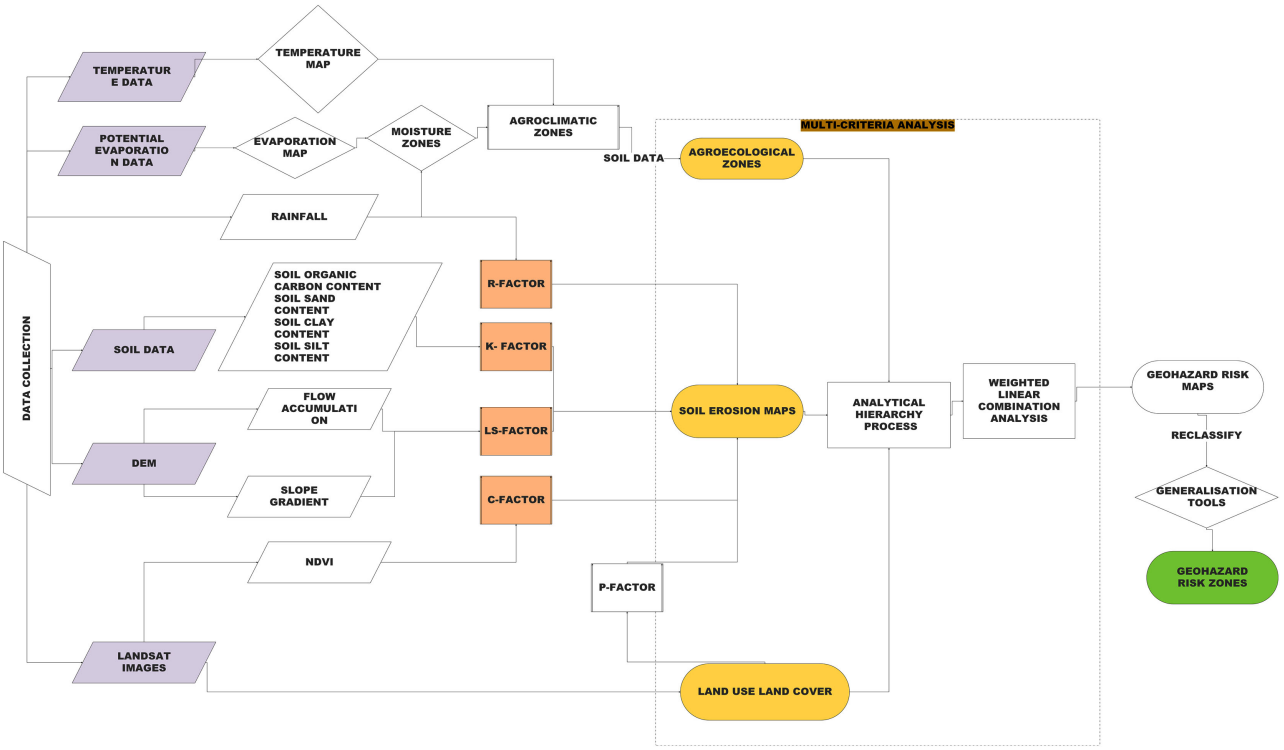

Figure 2. Methodology flowchart.

maps while potential evaporation data was used to generate moisture zones. Both outputs were combined to form agroclimatic zones over which soil data was overlayed to generate agroecological zones. Rainfall data, soil data, DEM and Landsat images were used to generate the RUSLE factors which were cross-multiplied to generate soil erosion maps. Landsat images were also used to create land use land cover maps using maximum likelihood classification algorithm. The detailed description is given in the sections and subsections below.

2.4.1. Land Use Land Cover

Land use land cover maps were developed using Landsat images for the years 1990, 2000, 2010 and 2020 as described.

Landsat images were downloaded from the USGS website and preprocessed through reprojection, haze reduction, layer stacking bands, mosaicking of the respective layer stacked tiles and subset using the area of interest polygon as the masking layer.

Subset images were then processed and classified using maximum likelihood algorithm in ENVI software. Each image was classified into six classes namely: forest, cropland, grassland, waterbody, bare land and built-up areas. Training sets were obtained using ArcMap and Google Earth Engine. The classified images depicted the changes in land use land cover over the given period of time.

2.4.2. Agroecological Zones Mapping

1) Temperature Maps

According to Balungi [4], temperature is closely related to altitude. Therefore,

temperature maps were developed by relating temperature to the respective altitude through generating a linear regression equation. The developed regression equations for the years 1990 and 2020 (Table 3 and Table 4).

$$y = 36.51468161409601 - 0.006114314933751732x \quad 1990 \tag{1}$$

$$y = 38.06396442796763 - 0.0067394482670173434x \quad 2020 \tag{2}$$

The equations were used in raster calculator to generate the temperature maps where the temperature data was the dependent value (y) and altitude served as the independent value (x). The maps obtained were reclassified to produce temperature zones maps.

2) Evaporation Maps

According to Rijks *et al.* [8], potential evaporation is related to elevation in a given area. The evaporation maps were developed similarly to the temperature maps using the regression equations shown below (Table 5 and Table 6).

Table 3. 1990 temperature data.

y (temp)	x (Alt)
27.65671921	1271
29.66995239	1112
29.93018532	1073
28.70175171	1269
22.05179405	2496
28.75625801	1130
29.96805573	1023
30.0301857	1051
28.47665024	1288

Table 4. 2020 temperature data.

y (temp)	x (Alt)
28.0425415	1271
30.05774117	1112
30.31994247	1073
29.09347534	1269
22.43669128	2496
29.14335251	1130
30.3573494	1023
30.42167854	1051
28.87034225	1288

Table 5. 1990 Potential evaporation data.

y (pet)	x (alt)
1279	1271
1324	1112
1372	1073
1321	1269
1139	2496
1319	1130
1335	1023
1367	1051
1311	1288

Table 6. 2020 Potential evaporation data.

y (pet)	x (alt)
1343	1271
1396	1112
1440	1073
1386	1269
1189	2496
1381	1130
1401	1023
1430	1051
1370	1288

$$y = 1494.928470409007 - 0.14421369431866246x \quad 1990 \tag{3}$$

$$y = 1573.4707574061877 - 0.15556508961625917x \quad 2020 \tag{4}$$

where evaporation was the dependent value and altitude was the independent value.

3) Moisture Availability Maps

Moisture availability maps were generated by calculating the ratio of rainfall data to the evaporation maps [4]. The maps obtained were then reclassified to generate moisture zones.

4) Agroclimatic Zones

A multiple overlay tool was used to obtain these maps by overlaying the temperature zones and moisture zones maps.

5) Agroecological Zones

Agroecological zones were created using an overlay cross-multiplication tool and multivariate geo-clustering analysis where agroclimatic zones maps were

overlayed with soil data to generate then geo-clustering analysis done to achieve the AEZ maps. These maps were then reclassified into different zones ranging from highly suitable for agriculture to unsuitable zones.

2.4.3. Soil Erosion Prediction

The RUSLE model which is based on the USLE model structure developed by Wischmeier and Smith [9] was used in this research to predict soil loss Kerio Valley. RUSLE model incorporates five parameters to calculate annual soil loss: rainfall and runoff erosivity, soil erodibility, slope length and steepness, cover management and support practice [10]. The equation below illustrates the model.

$$A = R * K * LS * C * P \tag{5}$$

where A is the annual soil loss, R is the rainfall erosivity factor, K is the soil erodibility factor, LS is the slope length and steepness factor, C is the cover management factor and P is the support practice factor.

1) R-Factor

According to Jiang *et al.* [11], this factor indicates the erosive power of rainfall and the runoff from the rainfall. Rainfall erosivity can be calculated using the equation developed by Kassam *et al.* [12] for use in Kenya. The greater the duration and intensity of a rainstorm the higher the rate of erosion [13].

$$R = 117.6\left(1.00105^{MAR}\right) \tag{6}$$

where MAR is the mean annual rainfall.

This equation was used to obtain R-factor maps for both years and resampled from near neighborhood to bilinear interpolation.

2) K-Factor

This factor serves as an index to assess the susceptibility of soil to erosion based on its properties [2]. In this research the factor was assessed suing the following soil properties; soil organic carbon content, soil clay content, soil sand content, soil silt content. The following equation developed by Kouli *et al.* [14] was used to calculate this factor.

$$\begin{aligned} K = & \left[0.2 + 0.3\exp^{\left(-0.0256SAND\left\{1-\frac{SILT}{100}\right\}\right)}\right] * \left[\frac{SILT}{CLAY + SILT}\right]^{0.3} \\ & * \left[1.0 - \frac{0.25CARBON}{CARBON + \exp^{(3.72-2.95CARBON)}}\right] \\ & * \left[1.0 - \frac{0.70\left(1-\frac{SAND}{100}\right)}{\left(1-\frac{SAND}{100}\right) + \exp^{\left(-5.51+22.9\left\{1-\frac{SAND}{100}\right\}\right)}}\right] \end{aligned} \tag{7}$$

3) LS-Factor

It is a combination of slope length and slope steepness [11]. Slope length was obtained from DEM as the flow accumulation raster while slope steepness was

obtained as slope in percentage using the Terrain Processing Toolset in ArcMap. The steeper and longer the slope the higher the rate of erosion [13]. LS factor was obtained using the equation given below as provided by Stone and Hilborn [13].

$$LS = \sqrt{\frac{fac * 30}{22.1}} * \left(0.0065 + 0.045s + 0.0065s^2\right) \quad (8)$$

where *fac* is flow accumulation and s the slope in percentage.

4) C-Factor

It is a ratio comparing the loss of soil from land under a specific crop to that in untilled and fallow land and is used to determine the effectiveness of soil and crop management systems in preventing soil loss [13]. In this study the method used to obtain *C* factor was proposed by Durigon *et al.* [15] and adopted by Colman [16] as shown below.

$$C = 0.1\left(\frac{-NDVI + 1}{2}\right) \quad \text{where } NDVI = \frac{NIR - RED}{NIR + RED} \quad (9)$$

Landsat images were used to calculate the *NDVI* maps using the Semi-Automatic Classification Plugin tool called band calculator on QGIS developed by Congedo [17].

5) P-Factor

It reflects the effects of practices that reduce the rate and amount of water runoff and thus reduce the amount of erosion [13]. In this research the p-factor value was assigned according to the land use land cover classes [18]. Cropland was assigned the value 0.5 and the other classes were assigned 1 as guided in the USDA Handbook No. 282 [9] (**Figure 3**).

2.4.4. Geohazard Risk Mapping

Geohazard risk assessment was done using the AHP tool for multi-criterion analysis. AHP is a method of organizing and analyzing complex decision problems using math and psychology [19] that was developed by Thomas Saaty [20]

S. no.	Land use/land cover classes	*P* values
1	Dense vegetation	1
2	Sparse vegetation	0.8
3	Built-up	1
4	Water bodies	1
5	Scrub land	1
6	Agricultural cropland	0.5
7	Fallow land	0.9
8	Bare soil/barren land	1

Source: USDA Handbook No. 282 (1981)

Figure 3. P-factor formula.

in the 1970s. The AHP is the most frequently used weighting method [21] and its main advantage is that it allows the breakdown of complex criteria into partial elements which are hierarchically related to each other [22]. The AHP uses pairwise comparison and linear algebra to calculate the weights of the different criteria. The higher the weight of a criterion, the more important it is in the final decision [23]. In this research AHP plugin tool in ArcMap developed by Oswald Marinoni [24] was used. It supports up to 15 criterion and can be used for risk mapping, spatial planning as well as suitability analysis [24].

Multi-criteria analysis techniques were used to generate geohazard maps from land use land cover maps, agroecological maps and soil erosion maps. AHP plugin in ArcMap was used to calculate the weights of the land use, soil loss and AEZ criterions using pairwise comparison and linear algebra algorithms. The assigned weights were used in multiple overlay tools to perform weighted overlay of the three datasets to generate the geohazard risk maps.

The risk maps were reclassified into five zones: very high risk, high risk, moderate risk, low risk and no risk. Generalization tools were then used to simplify and refine the risk zones as follows: Using the majority filter tool to remove misclassified cells, using the boundary clean tool to smooth the zones, and the region group tool to group clusters.

3. Results and Discussion

3.1. Land Use Land Cover Maps

Land use land cover maps of Kerio Basin were obtained for the years 1990, 2000, 2010, 2020 were obtained using maximum likelihood classification algorithm. The maps consisted of the following classes; forest, cropland, grassland, bare land, built-up area and waterbody. The area land use land cover changes are shown in the following table and figures (**Figure 4**).

Forested area decreased from approximately 18.91% in 1990 of the total area to 10.66% in 2020, whereas cropland decreased from approximately 30.96% in 1990 to 10.26% in 2020. Grassland coverage increased nearly double from 22.84% of the total area in 1990 to 43.36% in 2020, while bare land decreased slightly from 23.58% of the total area in 1990 to 21.17% in 2020. Built-up area increased tremendously from 2.84% of the total area in 1990 to 13.31% in 2020 (**Table 7**).

Decrease in forested area was caused by increased population which caused encroachment of forests in area thus reducing the forest coverage as more was converted in agricultural land and built-up. Agricultural expansion continues to be the main driver of deforestation and forest fragmentation and the associated loss of forest biodiversity [25].

Decreased cropland was caused by increased urbanization and population. More than 60% of the world's irrigated croplands are located near urban areas [26], which highlights the competition between urban areas and croplands for land [27]. According to Margaret Cunningham, around three million hectares of

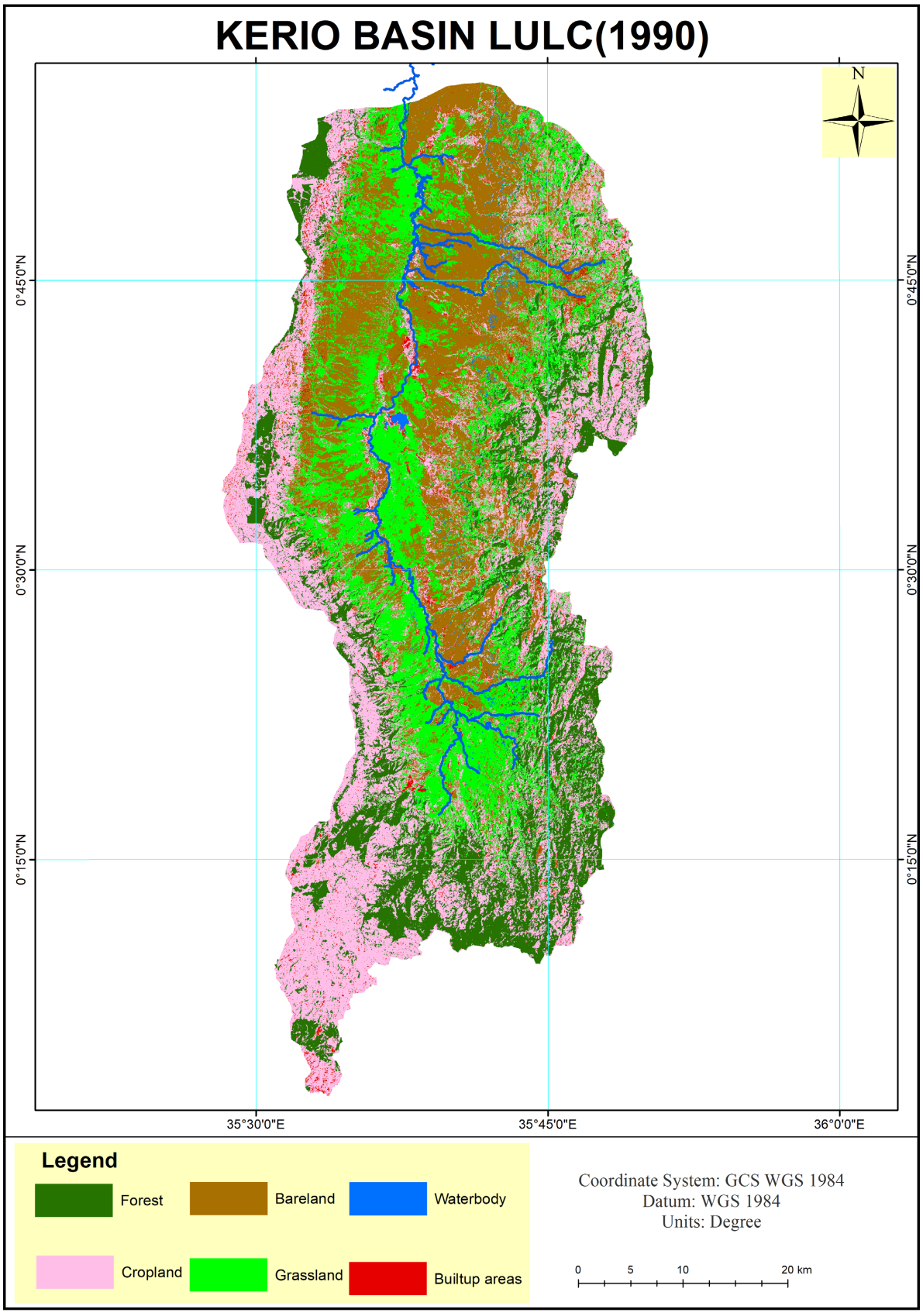
KERIO BASIN LULC(1990)
N
0°45'0"N
0°30'0"N
0°15'0"N
35°30'0"E
35°45'0"E
36°0'0"E
Legend
Forest
Bareland
Waterbody
Cropland
Grassland
Builtup areas
Coordinate System: GCS WGS 1984
Datum: WGS 1984
Units: Degree
0
5
10
20 km

(a)

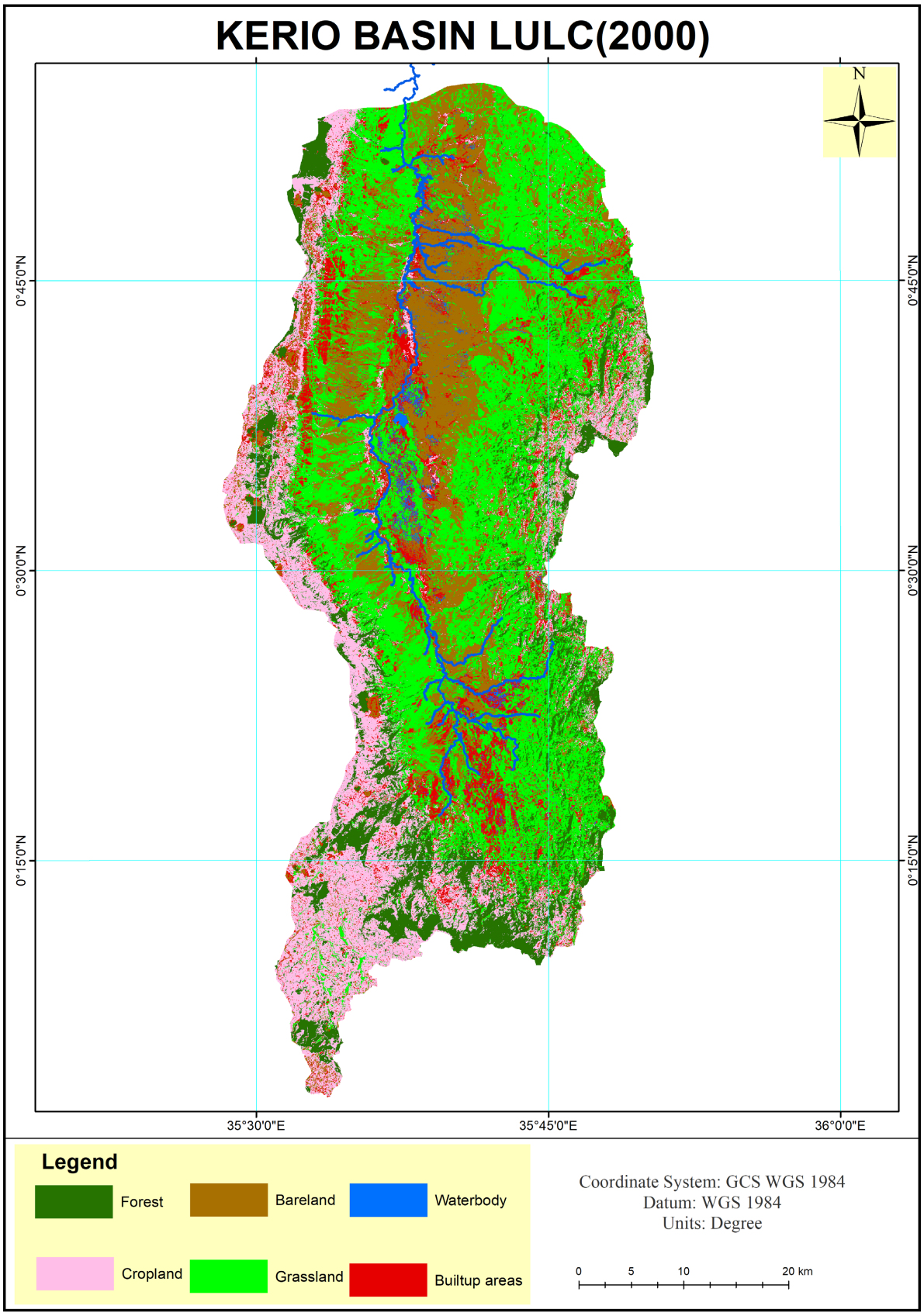
KERIO BASIN LULC(2000)
N
0°45'0"N
0°30'0"N
0°15'0"N
35°30'0"E
35°45'0"E
36°0'0"E
Legend
Forest
Bareland
Waterbody
Cropland
Grassland
Builtup areas
Coordinate System: GCS WGS 1984
Datum: WGS 1984
Units: Degree
0
5
10
20 km

(b)

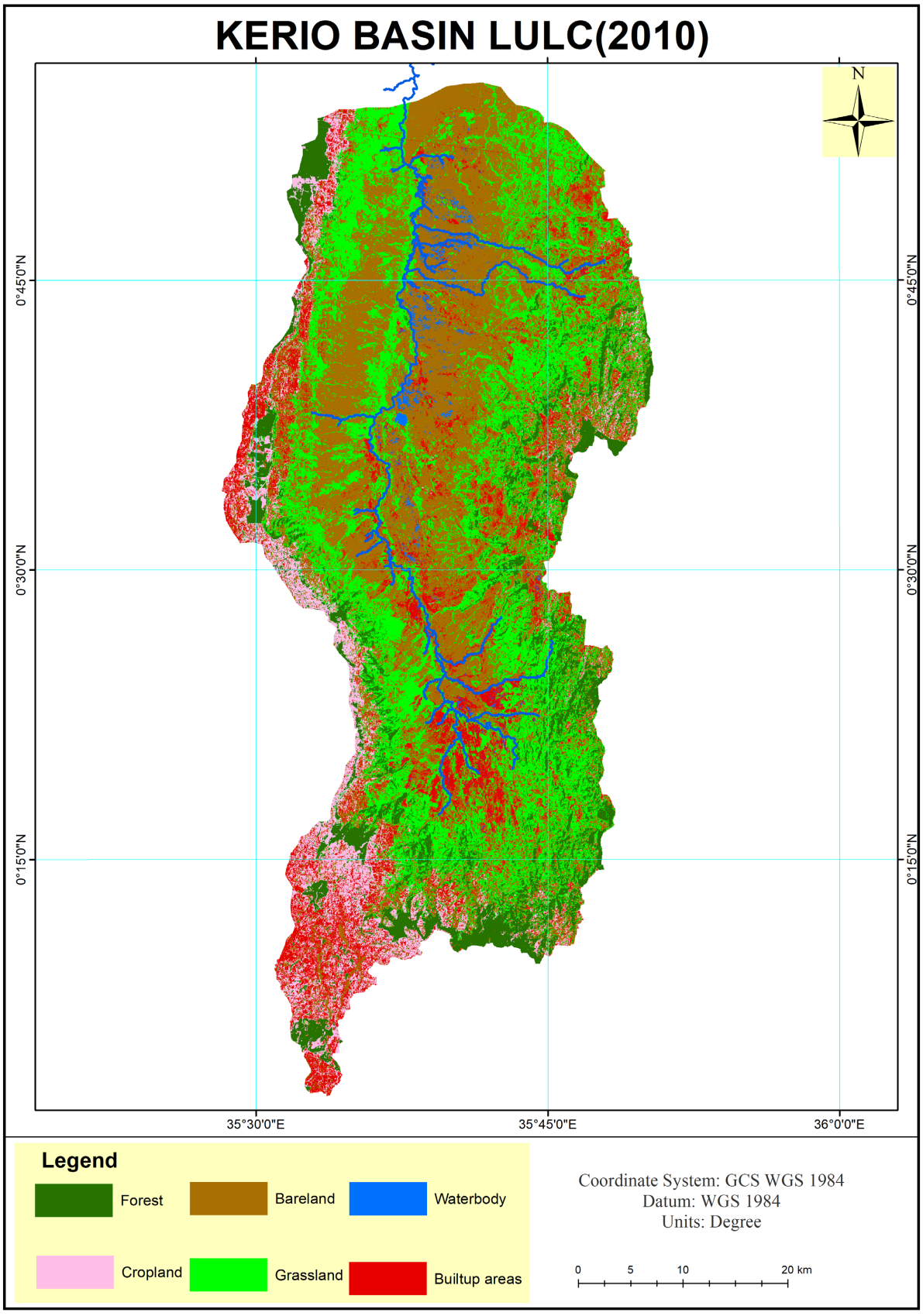
KERIO BASIN LULC(2010)
N
0°45'0"N
0°30'0"N
0°15'0"N
35°30'0"E
35°45'0"E
36°0'0"E
Legend
Forest
Bareland
Waterbody
Cropland
Grassland
Builtup areas
Coordinate System: GCS WGS 1984
Datum: WGS 1984
Units: Degree
0
5
10
20 km

(c)

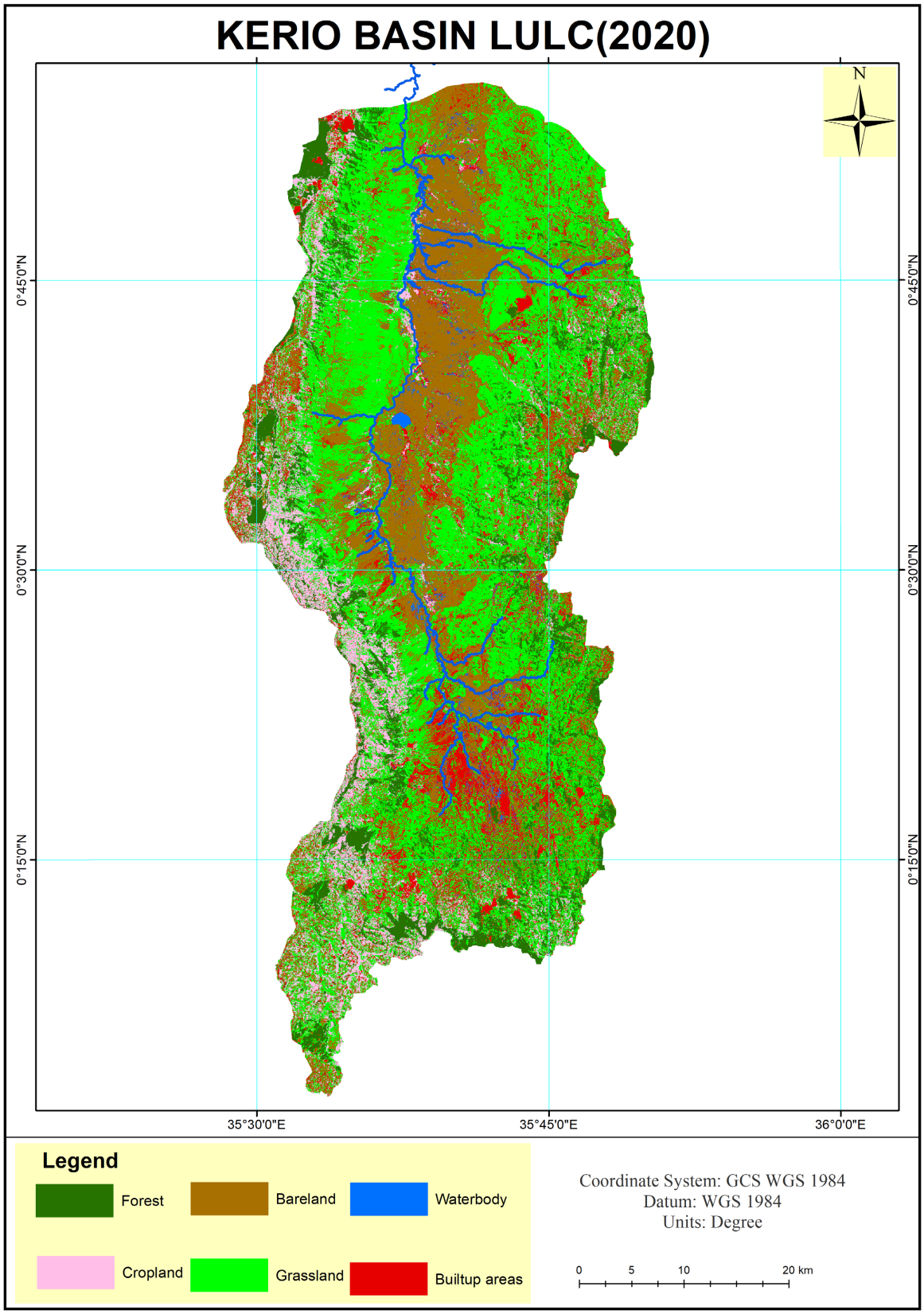

(d)

Figure 4. (a) 1990 lulc map, (b) 2000 lulc map, (c) 2010 lulc map, (d) 2020 lulc map.

Table 7. LULC class area in Ha and % of total.

CLASS	1990	90 area %	2000	00 area %	2010	10 area %	2020	2020 area %
Forest	46,330.29	18.91358253	29,590.58	12.07986105	26,964.99	11.00801714	26,120.7	10.66337216
Cropland	75,848.22	30.96379429	44,299.62	18.08458146	29,014.58	11.84472881	25,140.6	10.26326148
Grassland	55,944	22.83822228	93,133.08	38.02002752	72,474.03	29.58634008	106,214.49	43.36042432
Bareland	57,772.08	23.58450602	47,967.77	19.58204255	84,996.06	34.69825448	51,859.62	21.17088853
Built-up area	6958.26	2.840595748	27,203.13	11.10522439	29,295.43	11.95938124	32,613.11	13.31379822
Waterbody	2104.92	0.859299136	2763.77	1.128263035	2212.65	0.903278255	3008.7	1.228255285
	244,957.77		244,957.95		244,957.74		244,957.22	

agricultural land are lost each year because the soil degrades and becomes unusable due to erosion. An additional four million hectares are lost each year when agricultural land is converted and used for highways, housing, factories, and other urban needs [28].

The increase in grassland has been caused by deforestation where previously forested areas are left open thus resulting in grasslands as well as increased rainfall which resulted in previously bare areas to change to open grasslands.

Bare lands area has decreased due to increased conversion of barren land to built-up areas and croplands. Increased population growth has resulted in demand for more land in the area thus utilizing more barren land.

Built-up area has increased over the years as a result of increased population which has resulted in more settlements. Demand for social amenities, roads and other developments has increased exponentially with increase in population thus causing a high increase in built-up area.

Waterbodies area has increased as a result of changes in precipitation patterns where high rainfall was experienced throughout 2020 thus resulting in increased volumes of water. For instance, the area of Lake Kamnarok increased from 1.153 km^2 in 1990 to 1.84 km^2 in 2021.

3.2. Agroecological Zone Mapping

3.2.1. Temperature Maps

The temperature regression equations were used to create temperature maps for both years respectively, after which the maps were reclassified to generate temperature zones maps. The characteristics of the temperature zones are shown in Table 8.

From the maps, it was observed that colder conditions were experienced in 2020 than in 1990 as the lowest temperature decreased from 19.25˚C in 1990 to 19.04˚C in 2020.

Similarly, hotter conditions were experienced in 2020 than in 1990 as the highest recorded temperature increased from 30.27˚C in 1990 to 31.18˚C in 2020.

Table 8. Temperature zones properties.

Temperature Zones	1990 (˚C)	2020 (˚C)
High	28.23 - 30.27	28.93 - 31.18
Medium	25.67 - 28.23	26.11 - 28.93
Low	22.72 - 25.67	22.86 - 26.11
Very low	19.25 - 22.72	19.04 - 22.86

Higher temperatures were recorded in the lowland areas of the valley in both years while low temperatures were experienced in the highlands surrounding the valley. From the maps it was also observed that temperatures increased in the area at a rate of approximately 1˚C from 1990 to 2020.

It was also observed that areas near River Kerio and Lake Kamnarok have the highest temperatures and are classified a high temperature zone while areas on the edges of the basin where altitude is higher experience low temperatures and are classified as very low temperature zones.

3.2.2. Evaporation Maps

Evaporation regression data relating potential evaporation to altitude were used to generate evaporation maps for the years 1990 and 2020. High evaporation rates occur in the lowlands where the temperatures are higher while low evaporation rates occur on the high-altitude areas.

Higher evaporation rates were experienced in 2020 than in 1990 as shown in Figure 5 due to the increased amounts of rainfall received in 2020 than 1990 as well as increased temperatures in the region where temperature increased from a high of 30.27 in 1990 to a high of 31.18 in 2020 (Table 8).

The areas near River Kerio and Lake Kamnarok experience the highest temperatures in the basin thus have a higher evaporation rate as compared to areas on the slopes which experience lower temperatures thus have lower rates of evaporation (Figure 6).

3.2.3. Moisture Availability Maps

Rainfall maps and evaporation maps were used to generate the moisture availability maps which were then reclassified into three moisture zones (high, medium and low) as depicted in Table 9.

The moisture zones maps depicted that the lowland areas have a low moisture content while areas on the higher altitudes have a higher moisture content. This is attributed to high rainfall received on the slopes and low evaporation rates while the lower areas receive low amounts of rainfall while the evaporation rates are higher. The moisture content increased from 1990 to 2020 due to the change in precipitation patterns in 2020 when higher amounts of rainfall were experienced thus increasing the moisture content levels.

The centrally placed areas that border River Kerio and Lake Kamnarok have low moisture content while areas towards the edges of the basin where altitude is

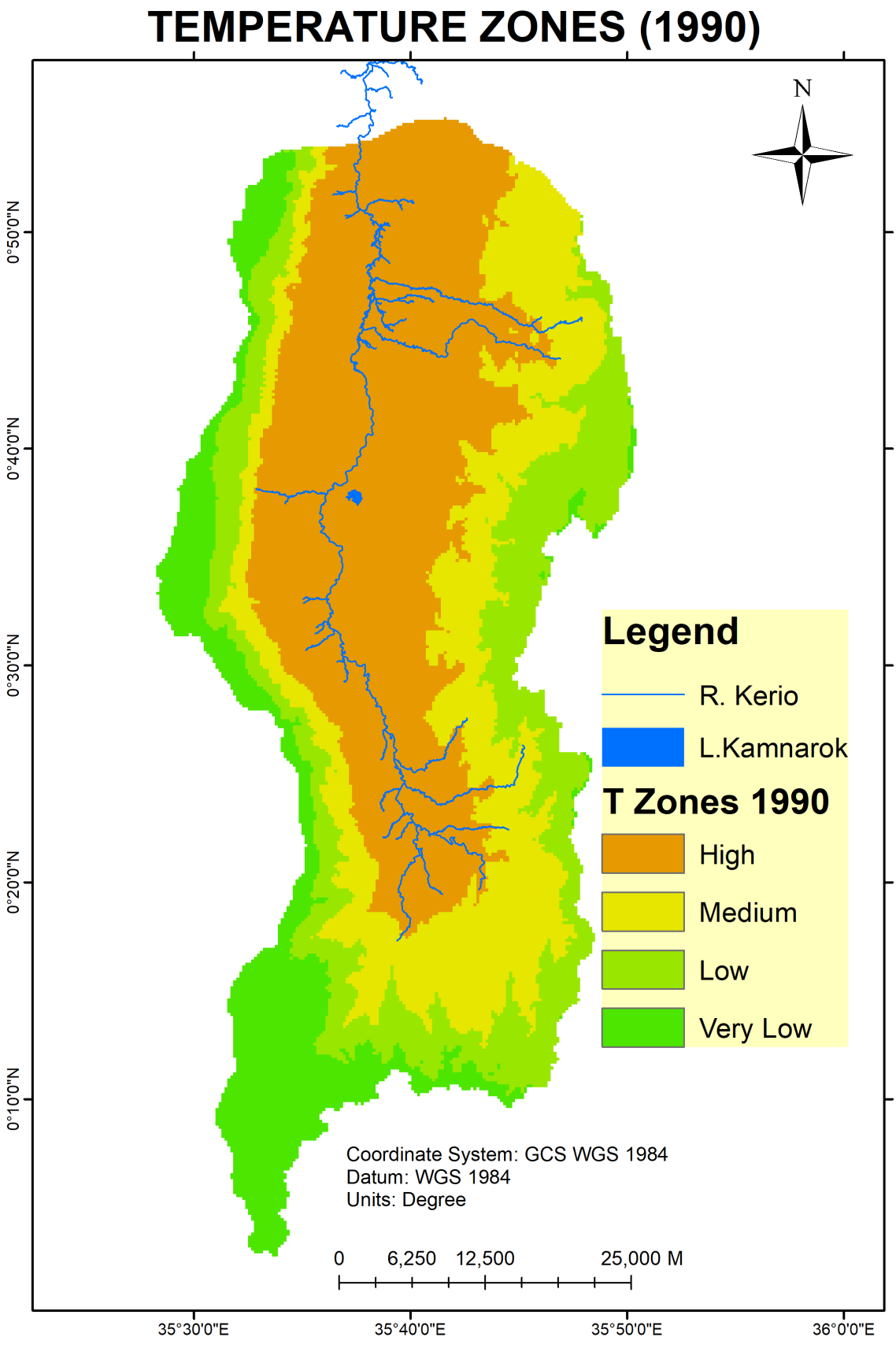
TEMPERATURE ZONES (1990)
N
0°50'0"N
0°40'0"N
0°30'0"N
0°20'0"N
0°10'0"N
35°30'0"E
35°40'0"E
35°50'0"E
36°0'0"E
Legend
R. Kerio
L.Kamnarok
T Zones 1990
High
Medium
Low
Very Low
Coordinate System: GCS WGS 1984
Datum: WGS 1984
Units: Degree
0 6,250 12,500 25,000 M

(a)

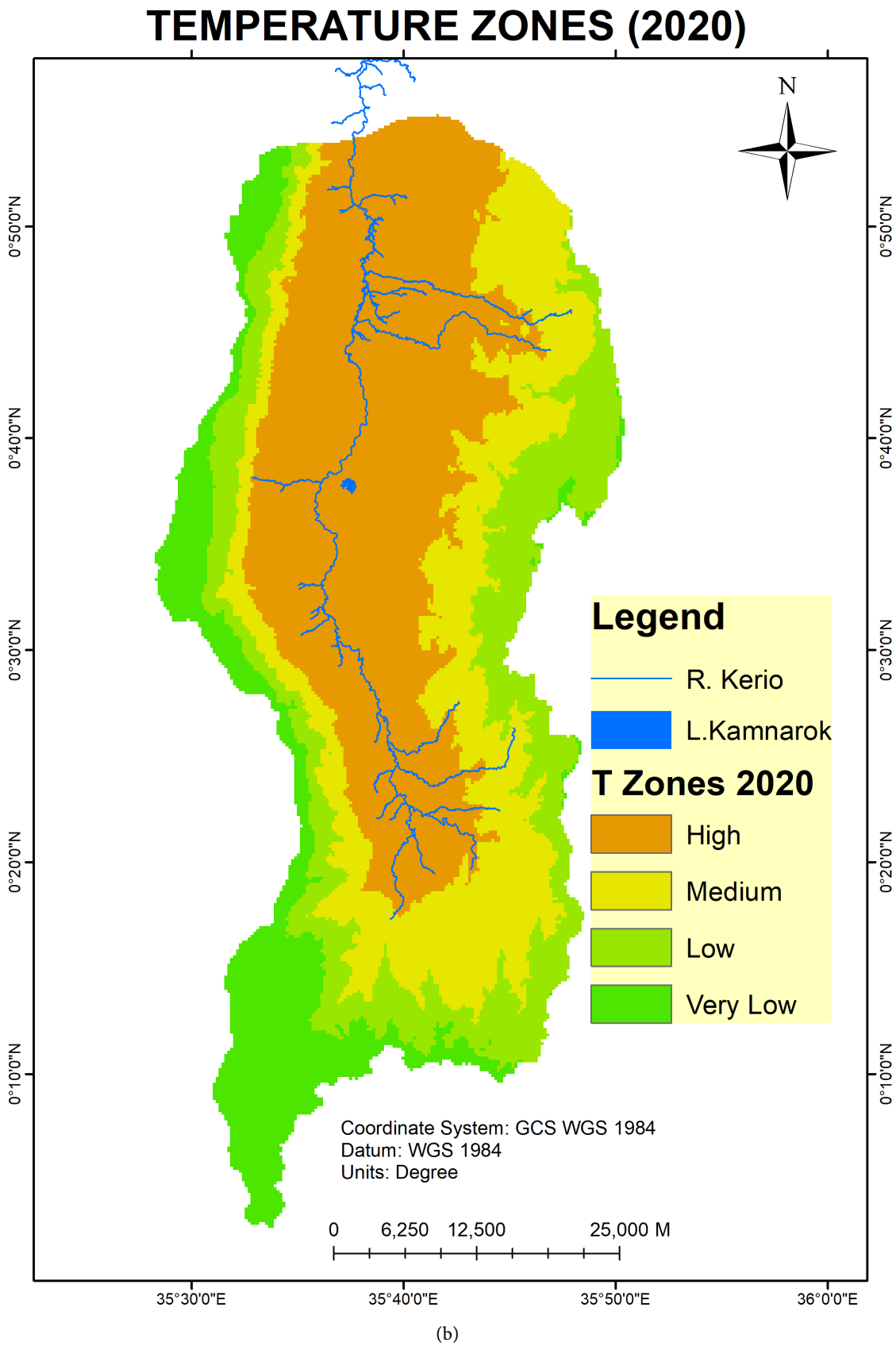

(b)

Figure 5. (a) 1990 Temperature zones, (b) 2020 Temperature zones.

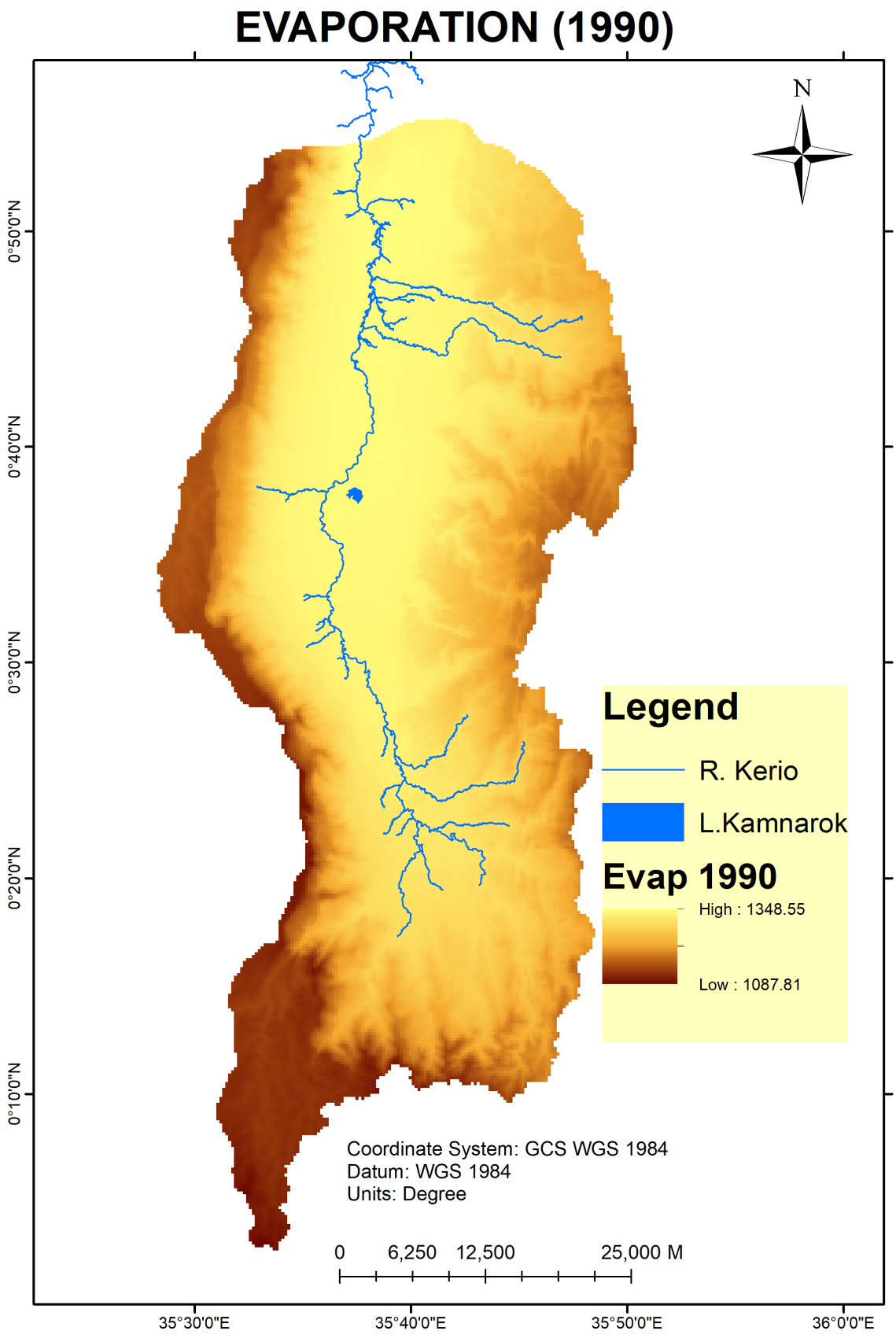
EVAPORATION (1990)
N
0°50'0"N
0°40'0"N
0°30'0"N
0°20'0"N
0°10'0"N
35°30'0"E
35°40'0"E
35°50'0"E
36°0'0"E
Legend
R. Kerio
L.Kamnarok
Evap 1990
High : 1348.55
Low : 1087.81
Coordinate System: GCS WGS 1984
Datum: WGS 1984
Units: Degree
0
6,250
12,500
25,000 M

(a)

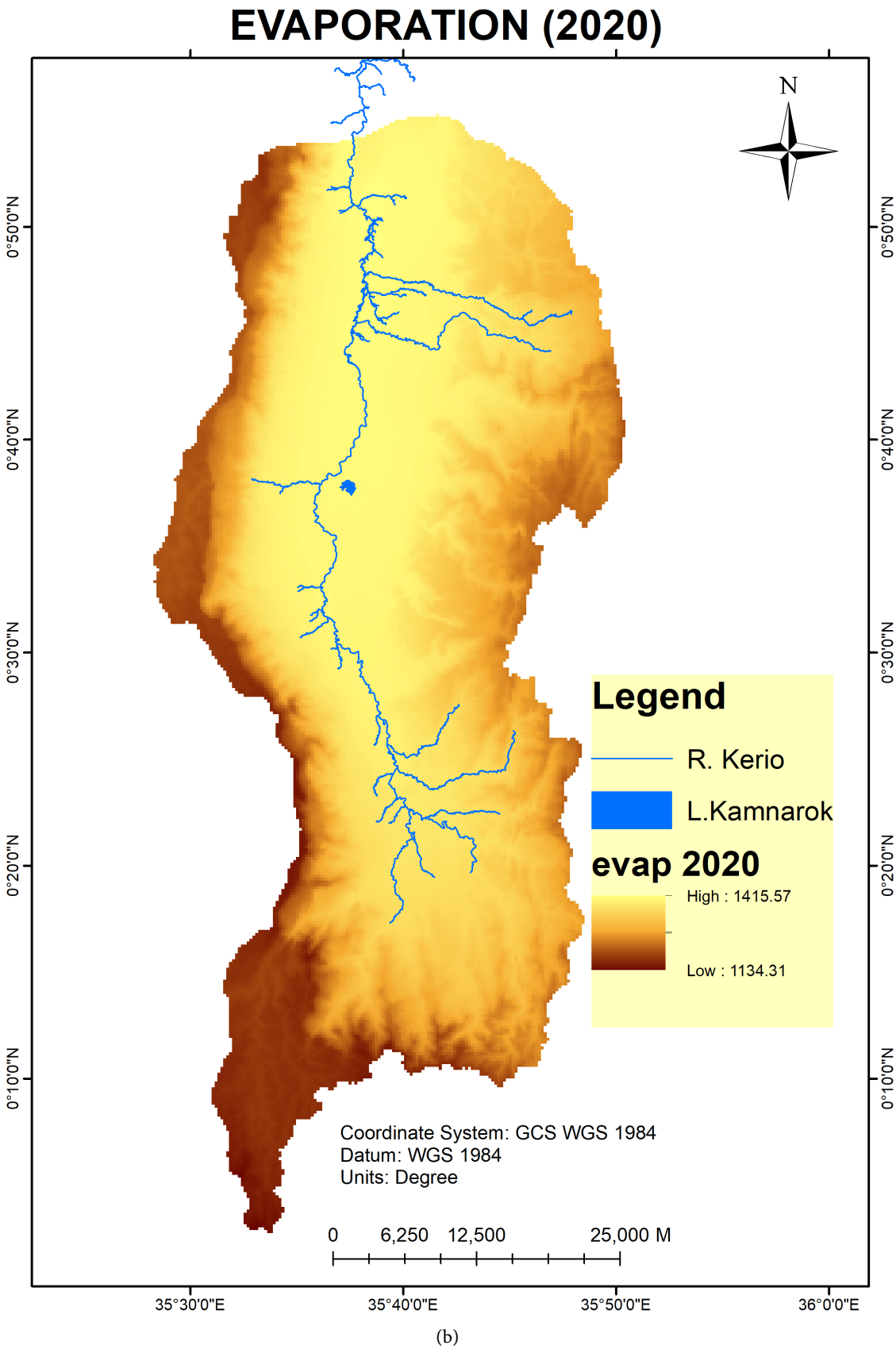

(b)

Figure 6. (a) 1990 evaporation map, (b) 2020 evaporation map.

Table 9. Moisture zone content.

Moisture Zones	Moisture Content	
	1990	2020
High	0.97 - 1.17	1.41 - 1.83
Medium	0.81 - 0.97	1.10 - 1.41
Low	0.65 - 0.81	0.83 - 1.10

higher have a higher moisture content. These moisture content zones can be used to determine the types of crops suitable for different areas in the basin. (Figure 7)

3.2.4. Agroclimatic Zones Maps

A weighted overlay analysis of moisture zone maps and temperature maps was used to obtain the agroclimatic maps which were reclassified into four agroclimatic zones; A1, A2, A3 and A4. The rainfall, temperature and moisture content characteristics are depicted in Table 10 and Table 11. (Figure 8)

3.2.5. Agroecological Zones Maps

Multivariate geo-clustering analysis of agroclimatic maps and soil maps was used to generate agroecological maps which were reclassified into five zones; Z1, Z2, Z3, Z4, Z5. Each zone had different characteristics that determine its suitability to agriculture. In this research, Principal Component Analysis tool in ArcMap was used generate agroecological maps. According to Boitt *et al.* [29], agroecological zones can be described as lowlands, upper lowlands, lower midlands, upper midlands and highlands as shown in Table 12. (Figure 9)

Lowlands decreased slightly (20% to 19%) in size from 1990 to 2020 as more land is put into agricultural use to cater for the increased demand for food which is an economic livelihood in the area. Higher amount of rainfall was received in 2020 thus allowing the transition of more land into arable land. Upper lowlands decreased from 25% to 20% between 1990 and 2020 while lower midlands increased from 19% to 23% between 1990 and 2020. Upper midlands also increased from 21% in 1990 to 24% in 2020 while highlands decreased slightly from 15% in 1990 to 14% in 2020. All figures are expressed as a percentage of the total area of the basin as shown in Table 13.

3.3. Soil Erosion Prediction

3.3.1. R-Factor

Equation (6) was used to generate R-factor maps in 1990 and 2020 using mean annual rainfall received in the area in both years. In 1990, the R-factor values ranged between 518.115 and 293.734, as the highest and lowest values respectively. In 2020, the values ranged from 1061.16 to 366.335 where the former was the highest value and the latter was the lowest value. Figure 10 below show the R-factor maps.

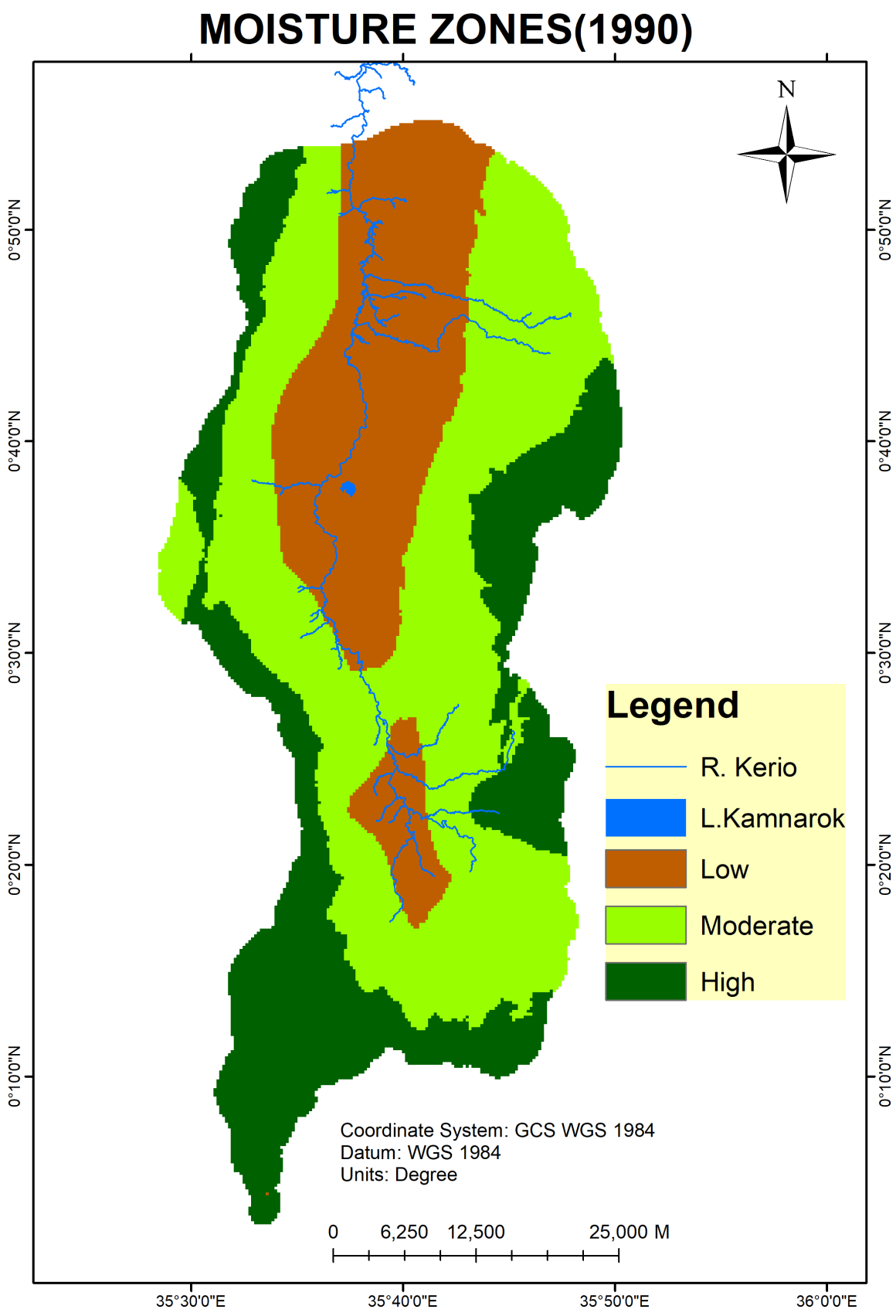
MOISTURE ZONES(1990)
N
0°50'0"N
0°40'0"N
0°30'0"N
0°20'0"N
0°10'0"N
35°30'0"E
35°40'0"E
35°50'0"E
36°0'0"E
Legend
R. Kerio
L.Kamnarok
Low
Moderate
High
Coordinate System: GCS WGS 1984
Datum: WGS 1984
Units: Degree
0
6,250
12,500
25,000 M

(a)

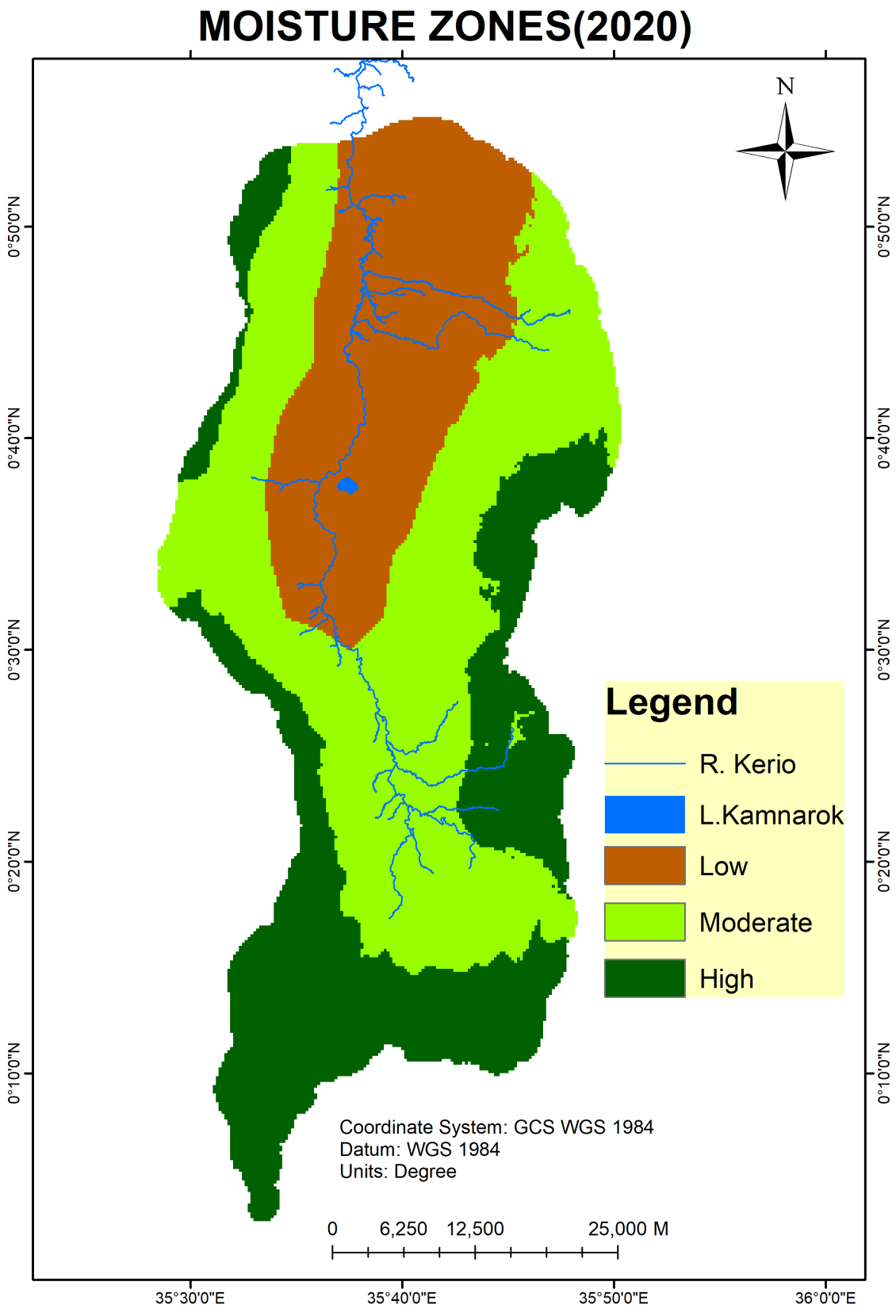

(b)

Figure 7. (a) 1990 Moisture zones, (b) 2020 Moisture zones.

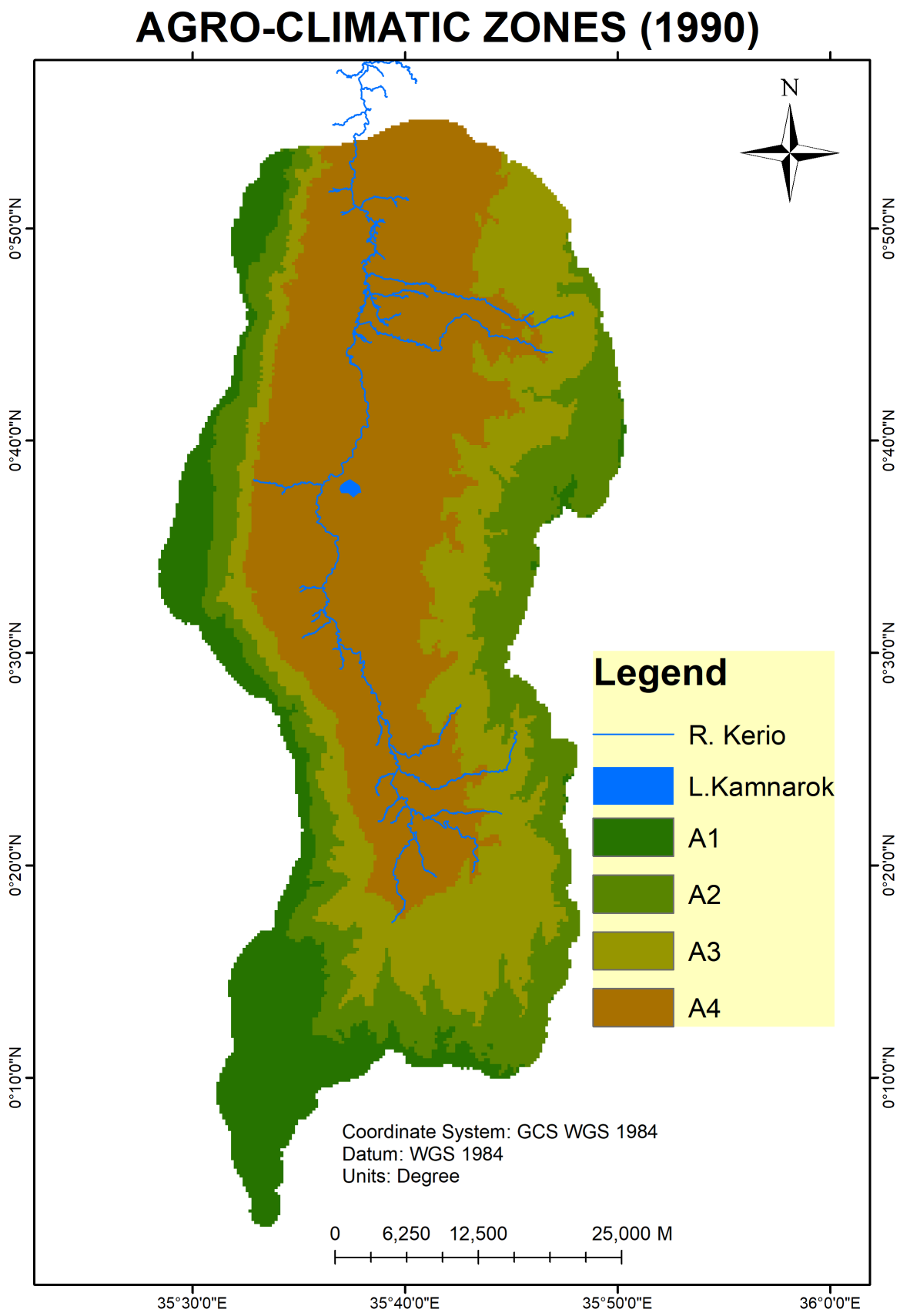
AGRO-CLIMATIC ZONES (1990)
N
0°50'0"N
0°40'0"N
0°30'0"N
0°20'0"N
0°10'0"N
35°30'0"E
35°40'0"E
35°50'0"E
36°0'0"E
Legend
R. Kerio
L.Kamnarok
A1
A2
A3
A4
Coordinate System: GCS WGS 1984
Datum: WGS 1984
Units: Degree
0
6,250
12,500
25,000 M

(a)

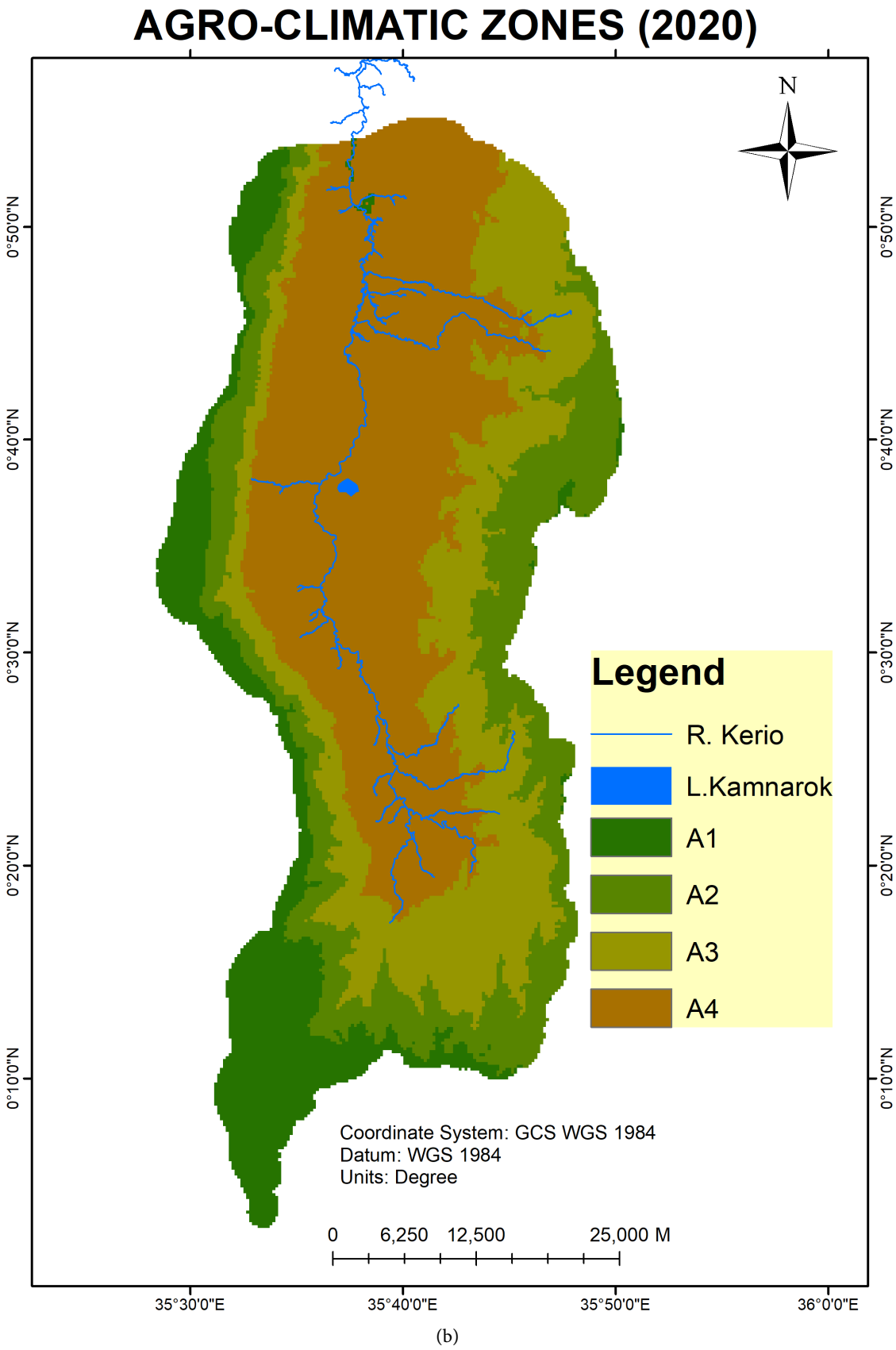

(b)

Figure 8. (a) 1990 agroclimatic zones, (b) 2020 agroclimatic zones.

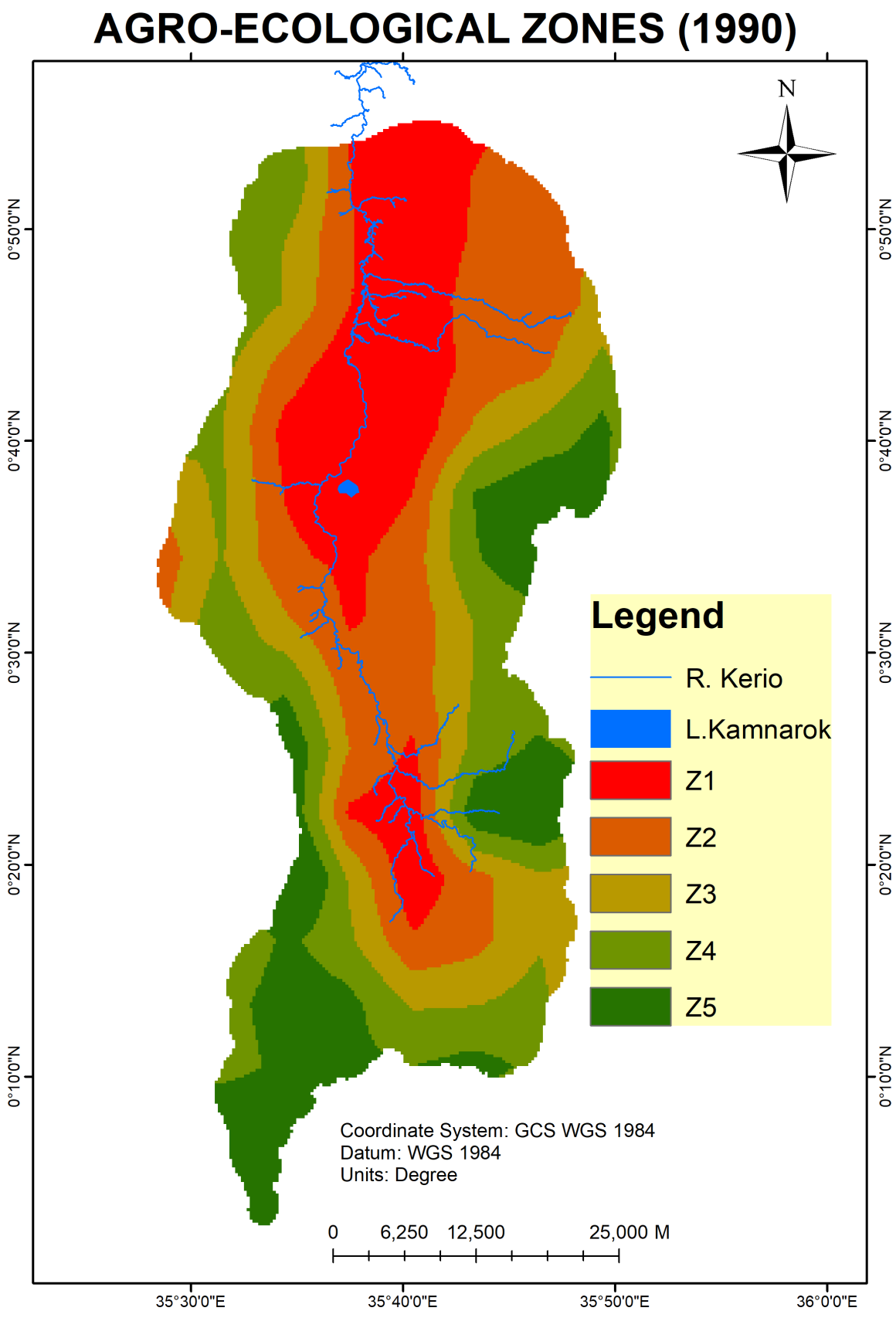
AGRO-ECOLOGICAL ZONES (1990)
N
0°50'0"N
0°40'0"N
0°30'0"N
0°20'0"N
0°10'0"N
35°30'0"E
35°40'0"E
35°50'0"E
36°0'0"E
Legend
R. Kerio
L.Kamnarok
Z1
Z2
Z3
Z4
Z5
Coordinate System: GCS WGS 1984
Datum: WGS 1984
Units: Degree
0 6,250 12,500 25,000 M

(a)

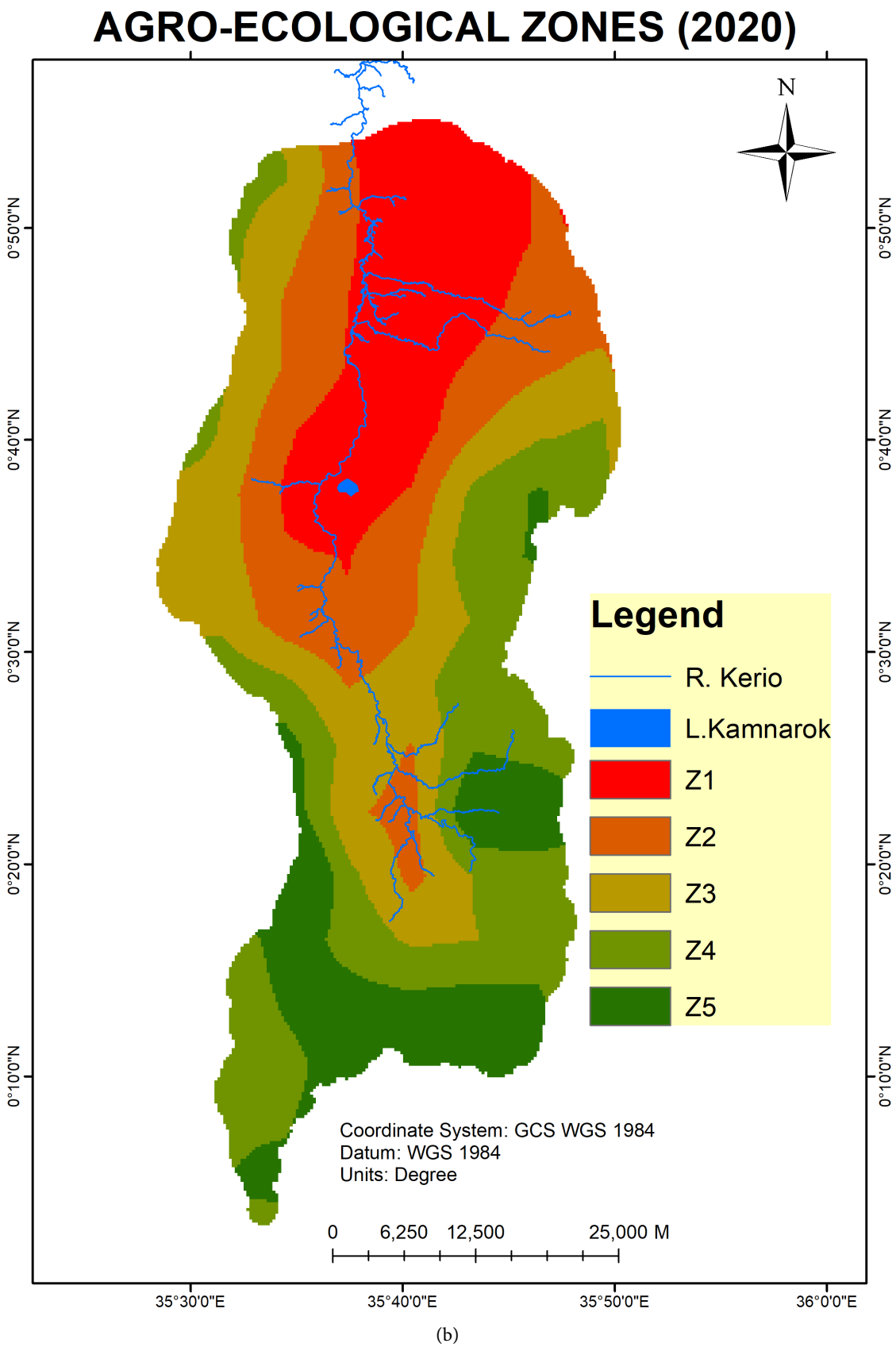

(b)

Figure 9. (a) 1990 agroecological zones, (b) 2020 agroecological zones.

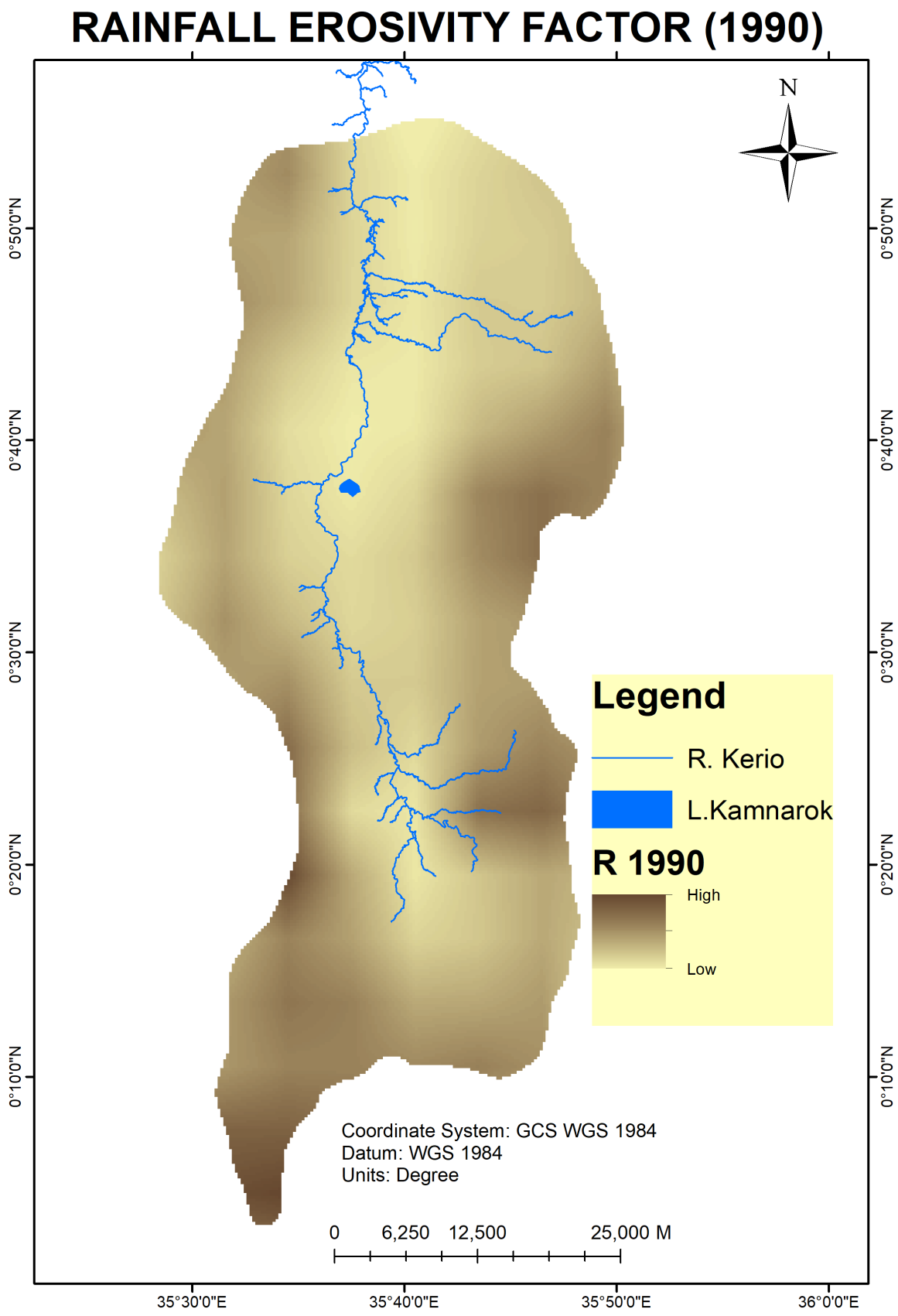
RAINFALL EROSIVITY FACTOR (1990)
N
0°50'0"N
0°40'0"N
0°30'0"N
0°20'0"N
0°10'0"N
35°30'0"E
35°40'0"E
35°50'0"E
36°0'0"E
Legend
R. Kerio
L.Kamnarok
R 1990
High
Low
Coordinate System: GCS WGS 1984
Datum: WGS 1984
Units: Degree
0 6,250 12,500 25,000 M

(a)

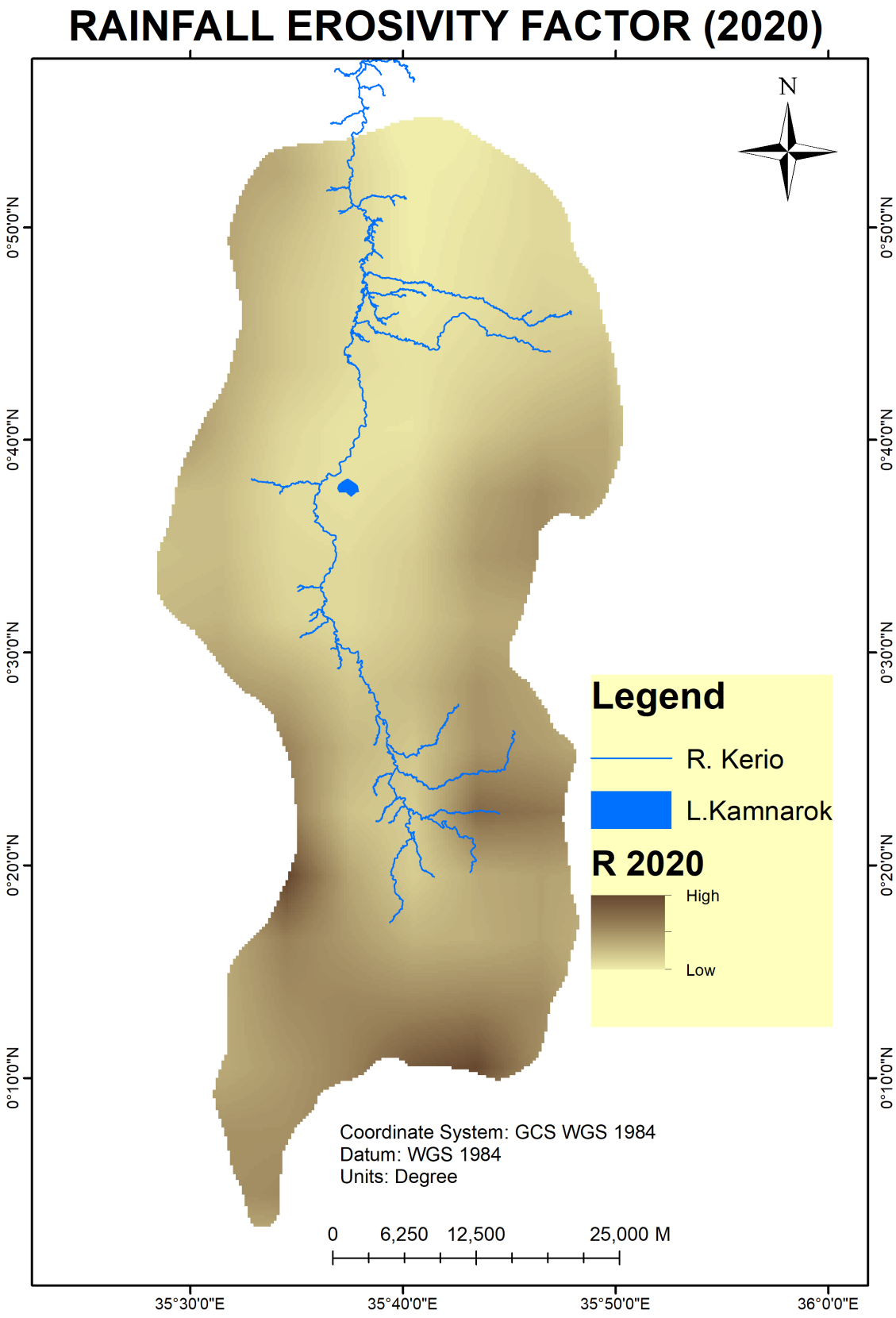

(b)

Figure 10. (a) 1990 R-factor, (b) 2020 R-factor.

Table 10. 1990 Agroclimatic zones characteristics.

Zone	Temperature (˚C)	Rainfall (mm)	Moisture Content
A1	28.23 - 30.27	872 - 982	0.64 - 0.82
A2	25.67 - 28.23	982 - 1078	0.82 - 0.97
A3	22.72 - 25.67	1078 - 1188	0.97 - 1.11
A4	19.25 - 22.72	1188 - 1410	1.11 - 1.30

Table 11. 2020 Agroclimatic zones characteristics.

Zone	Temperature (˚C)	Rainfall (mm)	Moisture Content
A1	28.93 - 31.18	1133 - 1397	0.79 - 1.09
A2	26.11 - 28.93	1397 - 1571	1.09 - 1.30
A3	22.86 - 26.11	1571 - 1737	1.30 - 1.48
A4	19.03 - 22.86	1737 - 2096	1.48 - 1.85

Table 12. Agroecological zones characteristics.

Zones	Description	Characteristics	
		Conditions	Crops
Z1	Lowlands	Higher temperatures Low rainfall	Typically, Sisal
Z2	Upper Lowlands	High temperatures Low rainfall	Sorghum, millet, early maturing maize and beans
Z3	Lower Midlands	Mid temperatures Average rainfall	Maize, cassavas, sweet potatoes
Z4	Upper Midlands	Low temperatures Above average rainfall	Maize, sugarcane, potatoes, tomatoes, agroforestry
Z5	Highlands	Lower temperatures Higher rainfall	Agroforestry, natural forests

Table 13. AEZ changes in percentage.

Zone	% Area in 1990	% area in 2020
Lowlands	20	19
Upper Lowlands	25	20
Lower Midlands	19	23
Upper Midlands	21	24
Highlands	15	14

3.3.2. K-Factor

K-factor is used to show the susceptibility of different soil types to erosion from rainfall and other erosive factors. Equation (7) was used to create the soil erodibility factor map by entering the it in a raster calculator on QGIS software. **Figure 11** shows the K-factor generated and used in this research. Soil properties remain unchanged over a long period of time which means that only one map was required for this study. Lowland areas of the map had the highest K factor

values which the highlands had the lowest K-factor values which means that the lowland soils are highly erodible while soils in the highlands have the lowest erodibility.

3.3.3. LS-Factor

LS-factor is used to calculate the susceptibility of land to erosion based on the steepness and length of a slope. In this research, Equation (8) was used to generate LS factor map and since elevation remains unchanged over the years only one map was required for the study. High elevation areas had a high LS factor value while low elevation areas had a low value. The map that was generated from the equation through a raster calculator is as shown in **Figure 11**.

3.3.4. C-Factor

C-factor maps were generated using Equation (9) for both years. The maps are as shown in **Figure 12**. In 1990, the values ranged from 0.076 to 0.012 while in 2020 the values ranged from 0.056 to 0.024.

3.3.5. P-Factor

P-factor maps were generated from land use land cover maps as shared in **Figure 13**.

3.3.6. Soil Loss Prediction

After obtaining all the required parameter maps, soil loss prediction maps were generated using Equation (5) where all factor maps were multiplied in a raster calculator separately for each year. (**Table 14** and **Figure 14** and **Figure 15**)

It was observed that the area near the slopes and highlands experienced the highest erosion rates due to steep slopes, longer slope length and high rainfall. The annual soil loss also increased from 1990 to 2020.

In 1990 the total predicted annual soil loss calculated in this research was 28.84 $t^{-1} \cdot ha^{-1} \cdot yr^{-1}$ while it was 78.81 $t^{-1} \cdot ha^{-1} \cdot yr^{-1}$ in 2020. The amount of eroded soil increased in 2020 due to increased loss of forest as shown in land use land cover analysis (**Table 7**). Increased rainfall due to changing precipitation patterns also resulted in increased R-factor values (**Figure 10**) thus increasing the amount of eroded soil.

Table 14. Soil loss.

1990		2020	
Erosion ($t^{-1} \cdot ha^{-1} \cdot yr^{-1}$)	Classification	Erosion ($t^{-1} \cdot ha^{-1} \cdot yr^{-1}$)	Classification
9.65 - 28.84	Very high	24.22 - 71.81	Severe
2.72 - 9.65	Moderate	5.63 - 24.22	High
1.47 - 2.72	Low	3.10 - 5.63	Moderate
0.56 - 1.47	Low	1.13 - 3.10	Low
0.01 - 0.56	Very low	0.04 - 1.13	Very low

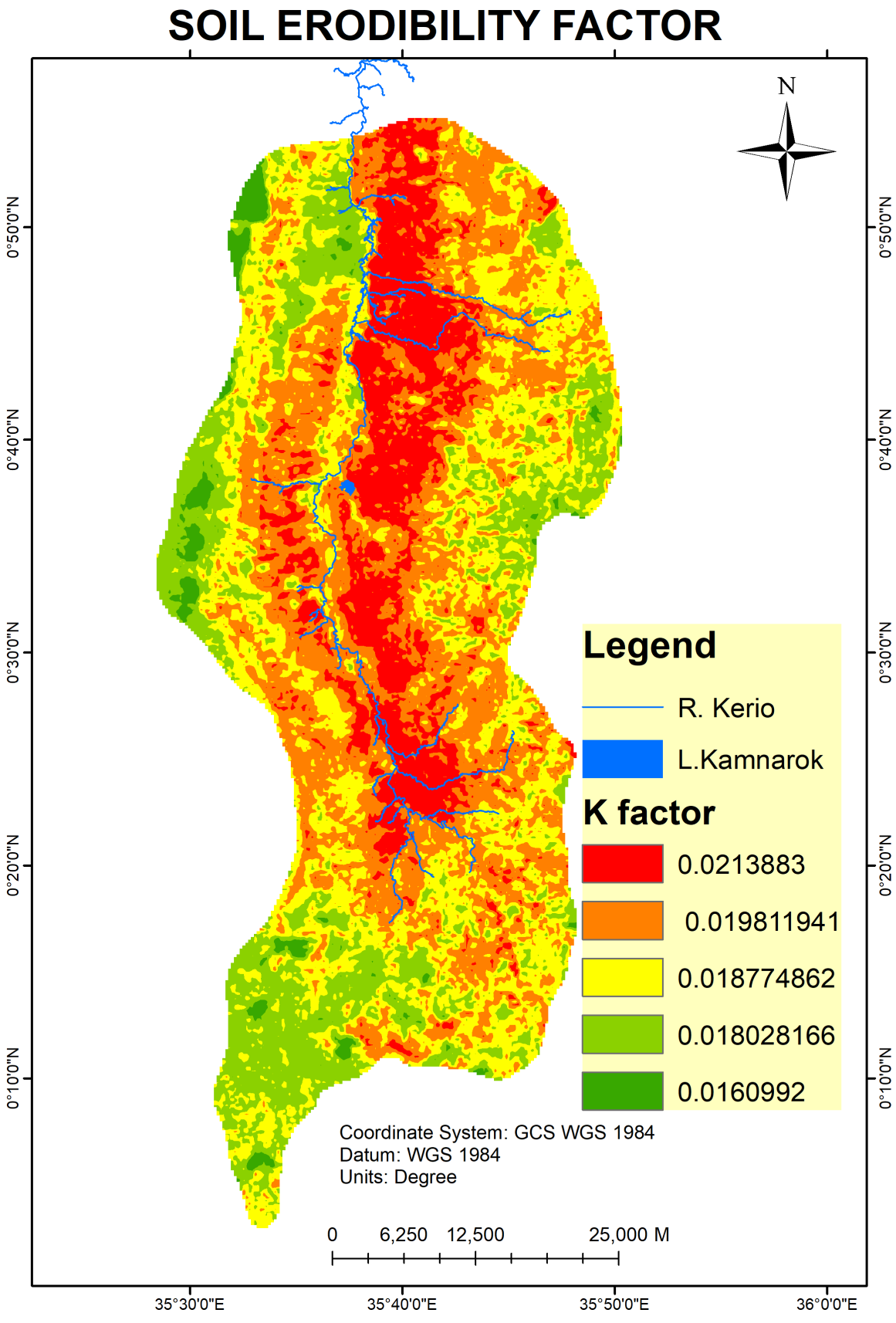
SOIL ERODIBILITY FACTOR
N
0°50'0"N
0°40'0"N
0°30'0"N
0°20'0"N
0°10'0"N
35°30'0"E
35°40'0"E
35°50'0"E
36°0'0"E
Legend
R. Kerio
L.Kamnarok
K factor
0.0213883
0.019811941
0.018774862
0.018028166
0.0160992
Coordinate System: GCS WGS 1984
Datum: WGS 1984
Units: Degree
0 6,250 12,500 25,000 M

(a)

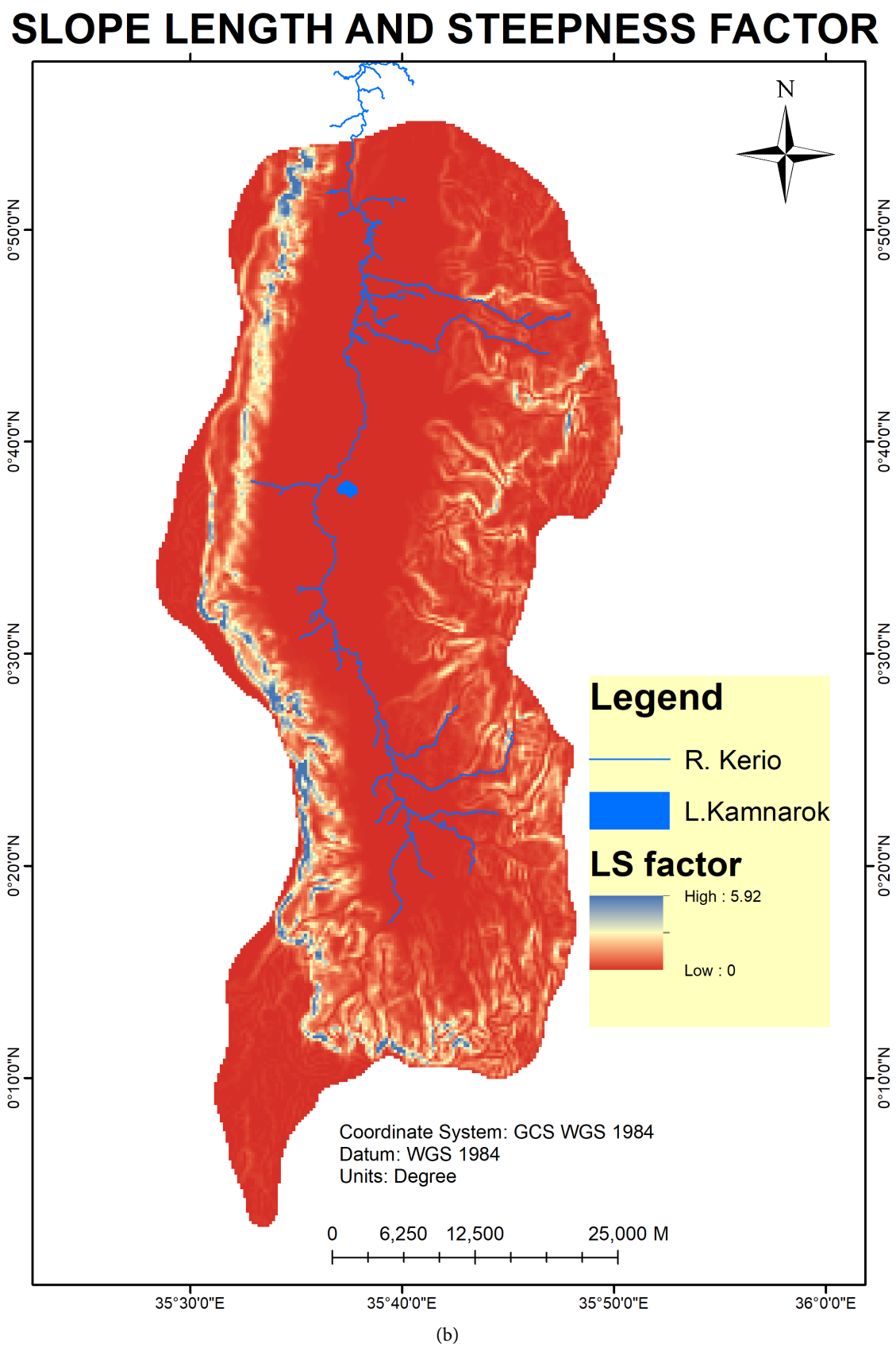

(b)

Figure 11. (a) K-factor, (b) LS-factor.

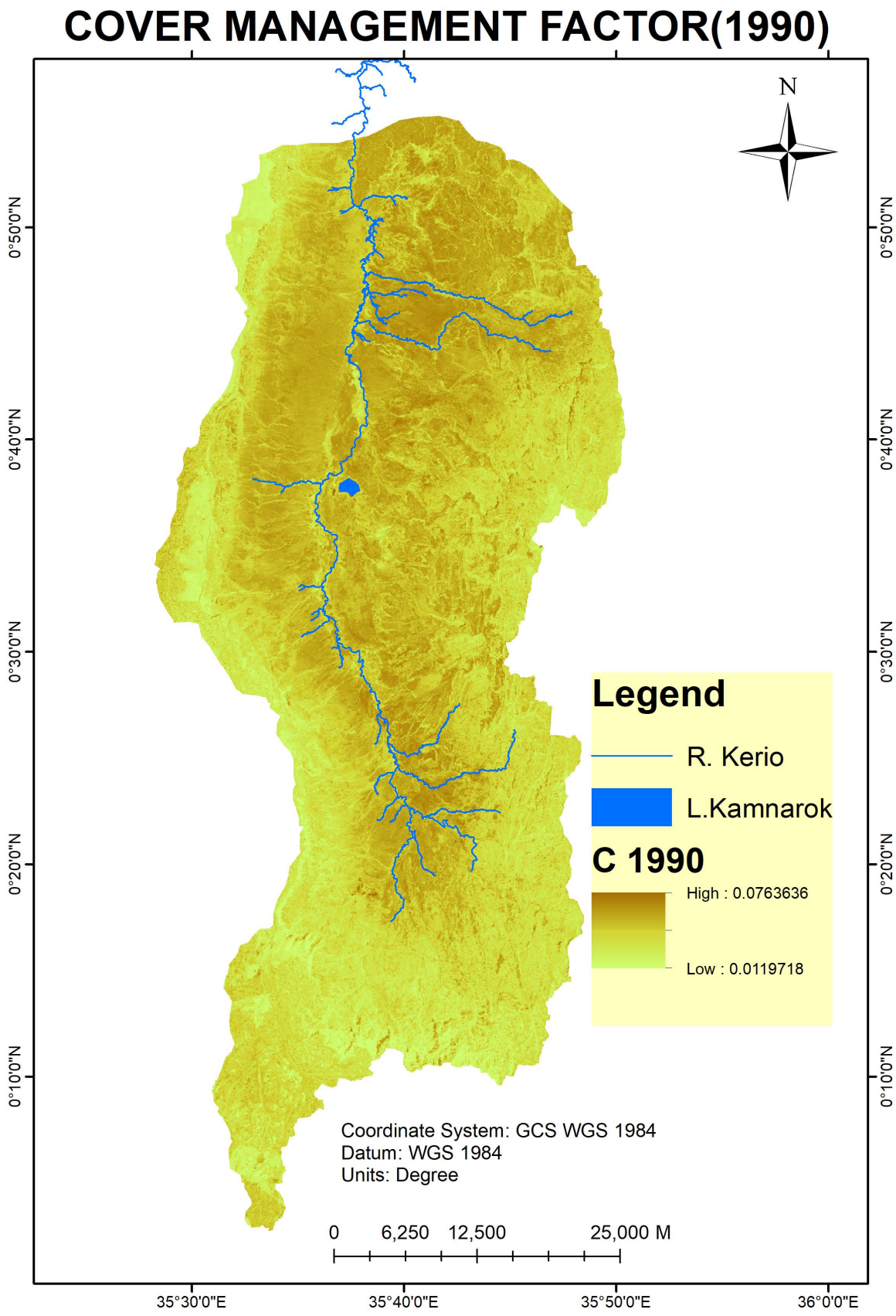
COVER MANAGEMENT FACTOR(1990)
N
0°50'0"N
0°40'0"N
0°30'0"N
0°20'0"N
0°10'0"N
35°30'0"E
35°40'0"E
35°50'0"E
36°0'0"E
Legend
R. Kerio
L.Kamnarok
C 1990
High : 0.0763636
Low : 0.0119718
Coordinate System: GCS WGS 1984
Datum: WGS 1984
Units: Degree
0 6,250 12,500 25,000 M

(a)

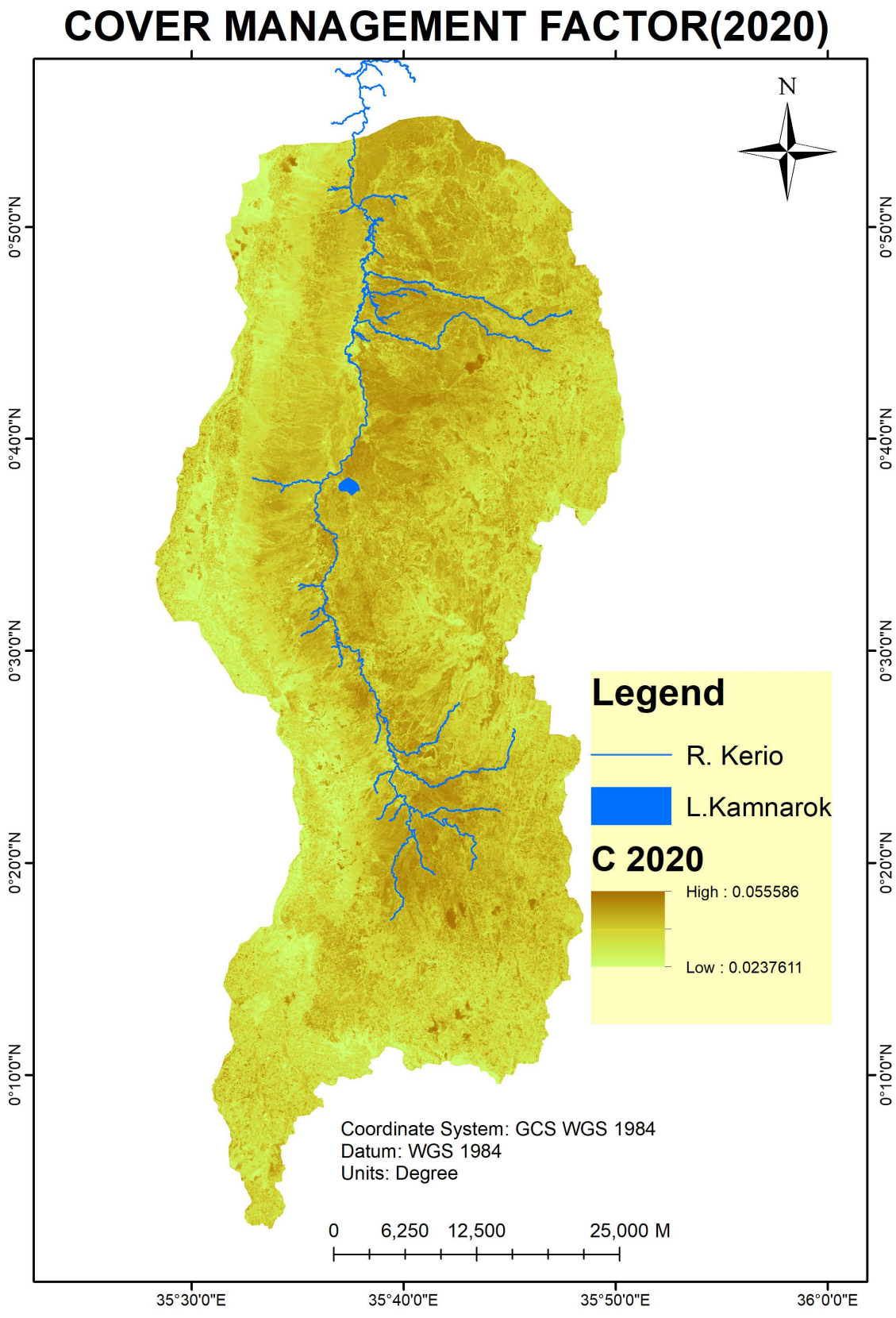

(b)

Figure 12. (a) 1990 C-factor, (b) 2020 C-factor.

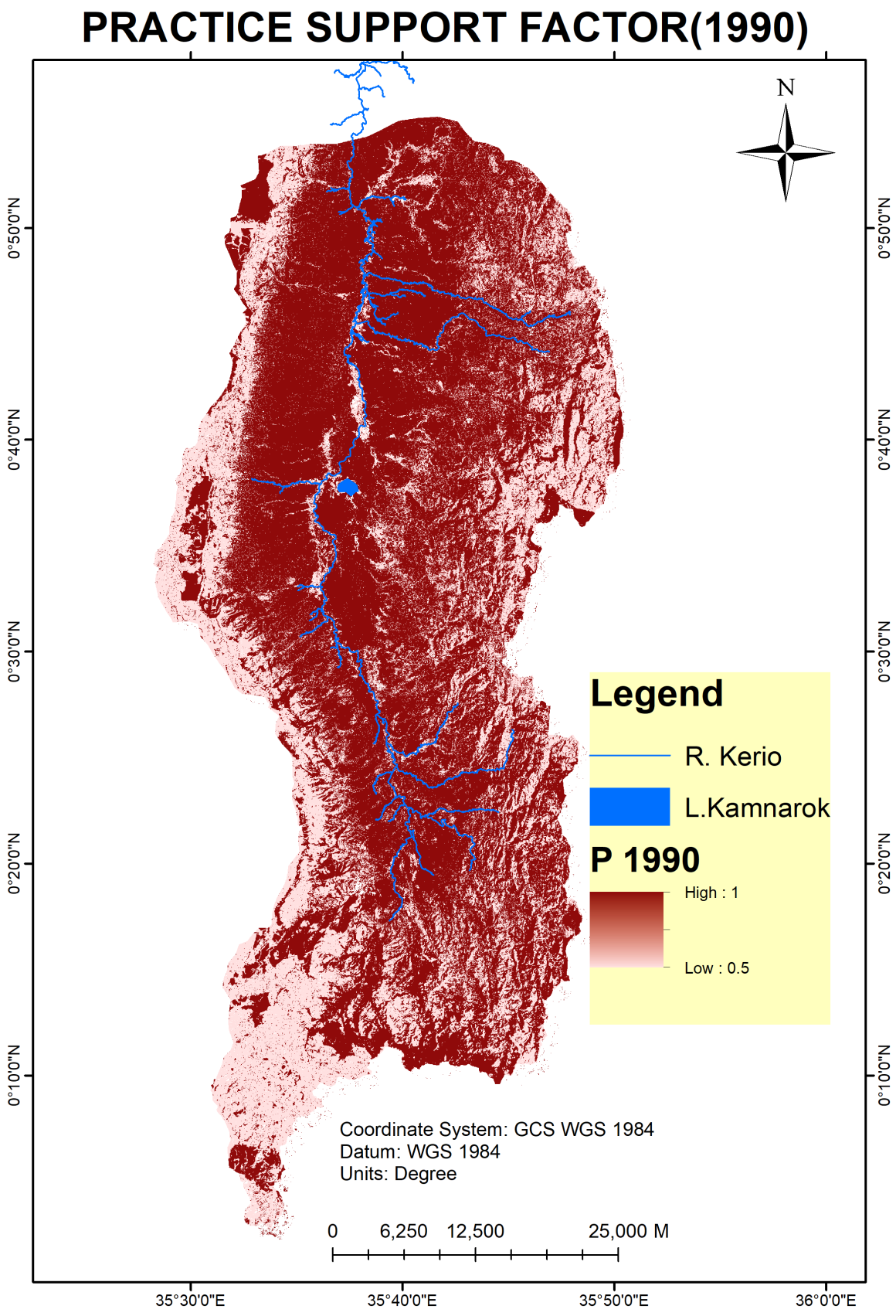
PRACTICE SUPPORT FACTOR(1990)
N
0°50'0"N
0°40'0"N
0°30'0"N
0°20'0"N
0°10'0"N
35°30'0"E
35°40'0"E
35°50'0"E
36°0'0"E
Legend
R. Kerio
L.Kamnarok
P 1990
High : 1
Low : 0.5
Coordinate System: GCS WGS 1984
Datum: WGS 1984
Units: Degree
0 6,250 12,500 25,000 M

(a)

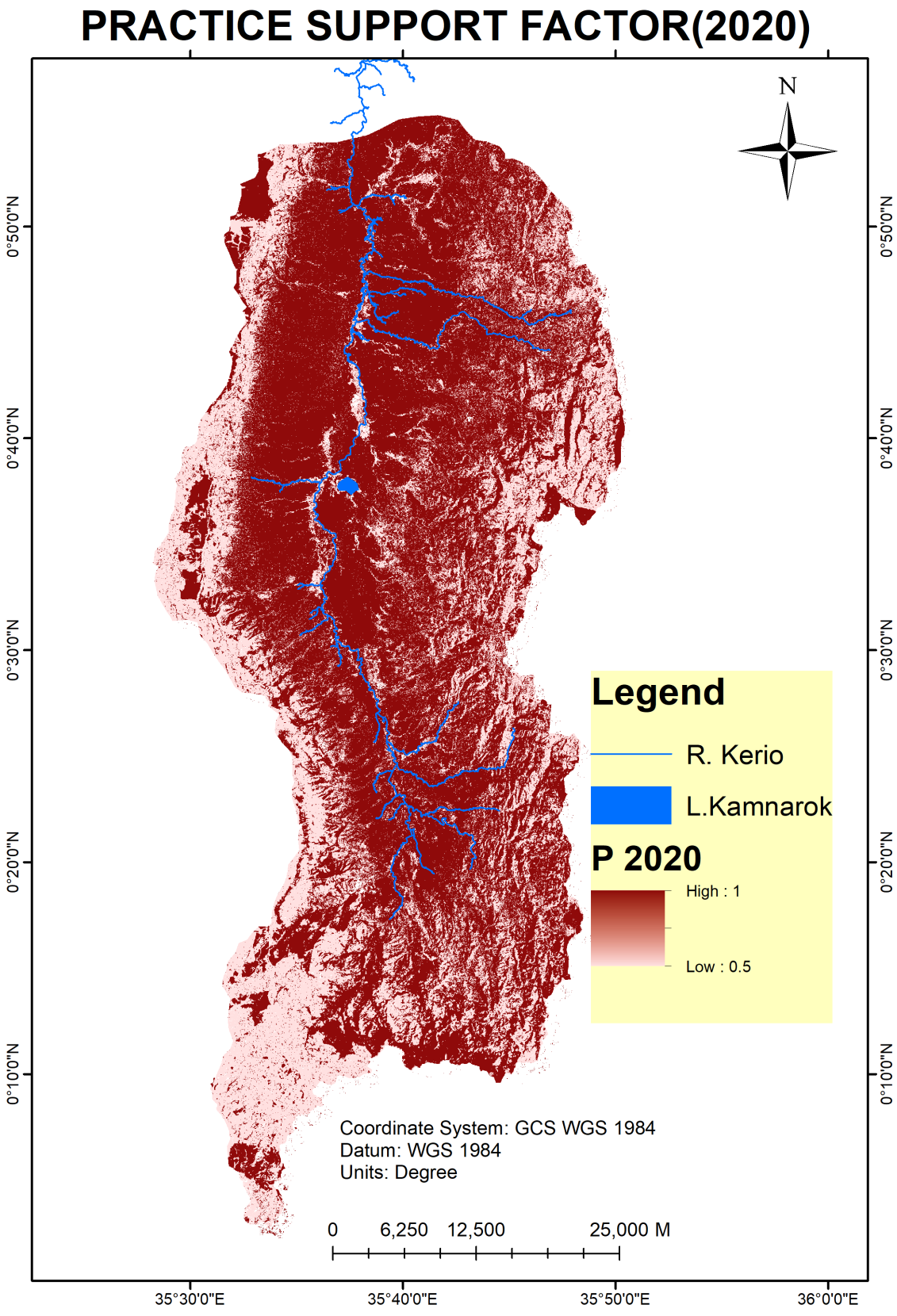

(b)

Figure 13. (a) 1990 P-factor, (b) 2020 P-factor.

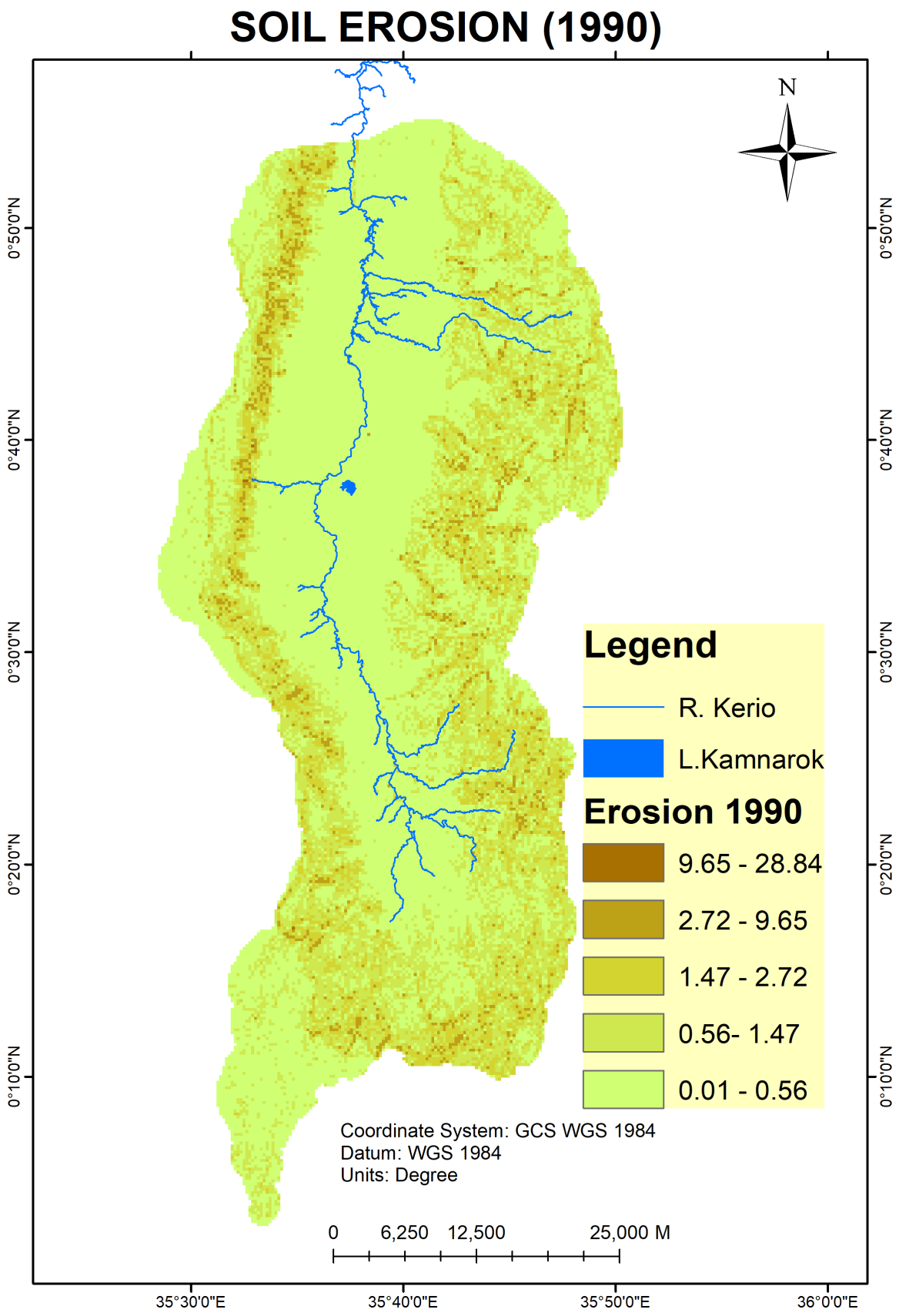
SOIL EROSION (1990)
N
0°50'0"N
0°40'0"N
0°30'0"N
0°20'0"N
0°10'0"N
35°30'0"E
35°40'0"E
35°50'0"E
36°0'0"E
Legend
R. Kerio
L.Kamnarok
Erosion 1990
9.65 - 28.84
2.72 - 9.65
1.47 - 2.72
0.56- 1.47
0.01 - 0.56
Coordinate System: GCS WGS 1984
Datum: WGS 1984
Units: Degree
0 6,250 12,500 25,000 M

(a)

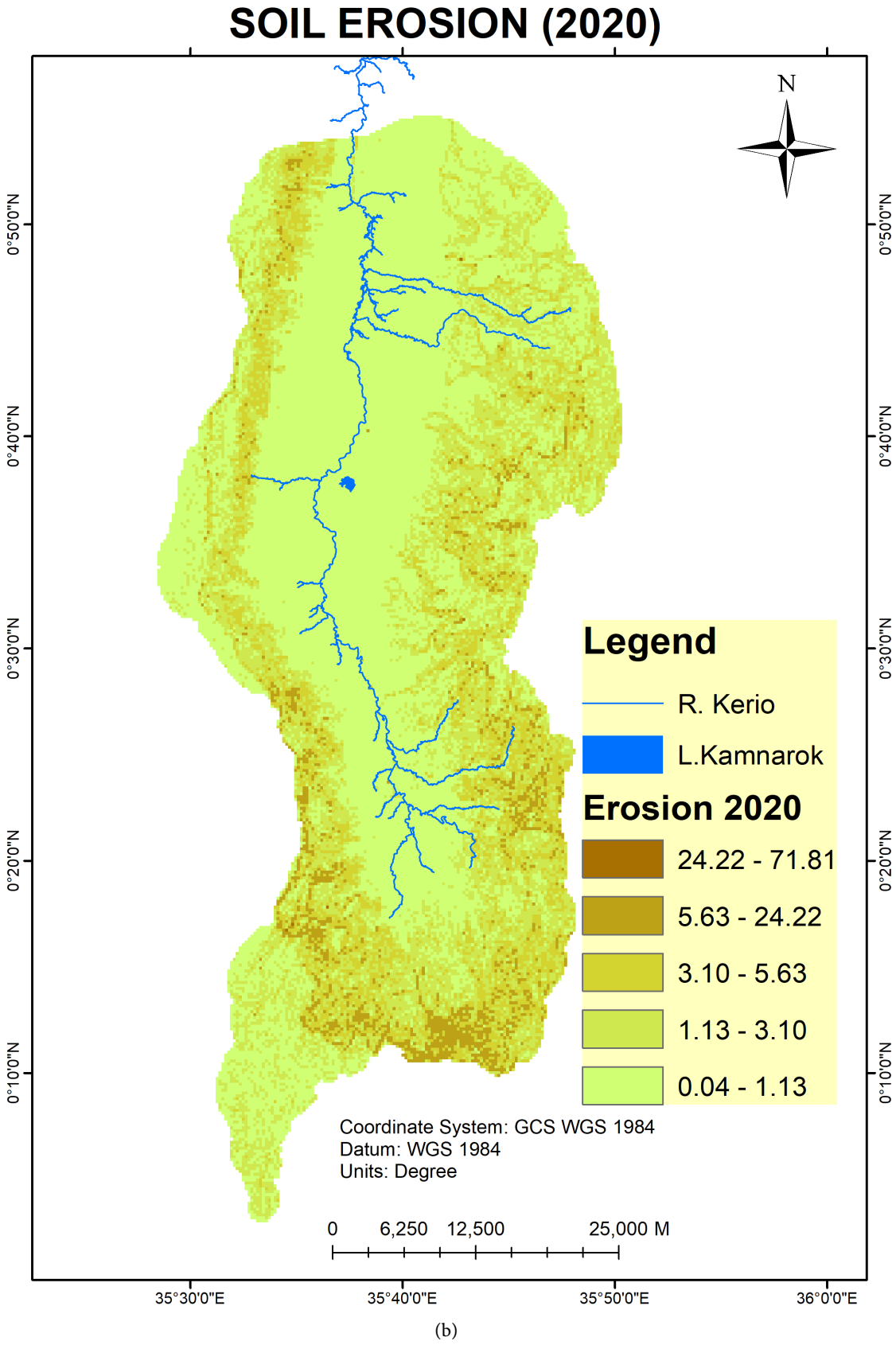

(b)

Figure 14. (a) 1990 Soil erosion prediction, (b) 2020 Soil erosion prediction.

3.4. Geohazard Risk Mapping

In this research, pairwise comparison was done through Analytical Hierarchy Process in ArcMap and expert opinion to generate weights of AEZ maps, soil erosion maps and land use land cover maps. The calculated weights were used in multiple overlay analysis to generate geohazard risk maps. The risk maps were divided into five zones namely; Very high-risk zones, high risk zones, moderate risk zones, low risk zones and no risk zones.

In 1990, these zones occupied 49.49%, 8.72%, 9.17%, 22.04% and 10.58% of the total area respectively. In 2020, these zones occupied 61.53%, 8.92%, 5.20%, 10.20% and 14.15% respectively as shown in Figure 16.

Very high-risk zone increased from 49.49% coverage in 1990 to 61.53% in 2020 while the high-risk remained relatively the same. Moderate risk zone reduced from a coverage of approximately 8.72% to 5.2% while the no risk zone increased from 10.57% coverage to 14.15% coverage. The low-risk zone decreased in size from 22.04% coverage in 1990 to 10.2% coverage in 2020. The geohazard risk zone maps are shown in Figure 17.

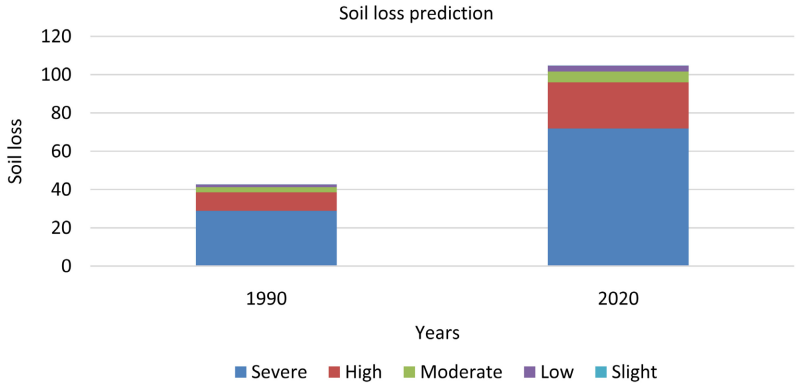

Figure 15. 1990 and 2020 soil loss bar graph.

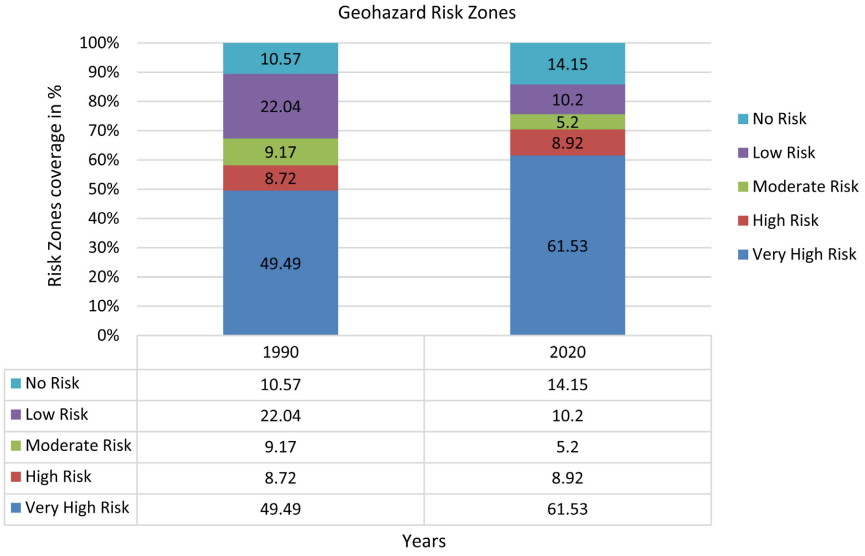

Figure 16. A bar graph showing Geohazard risk zones.

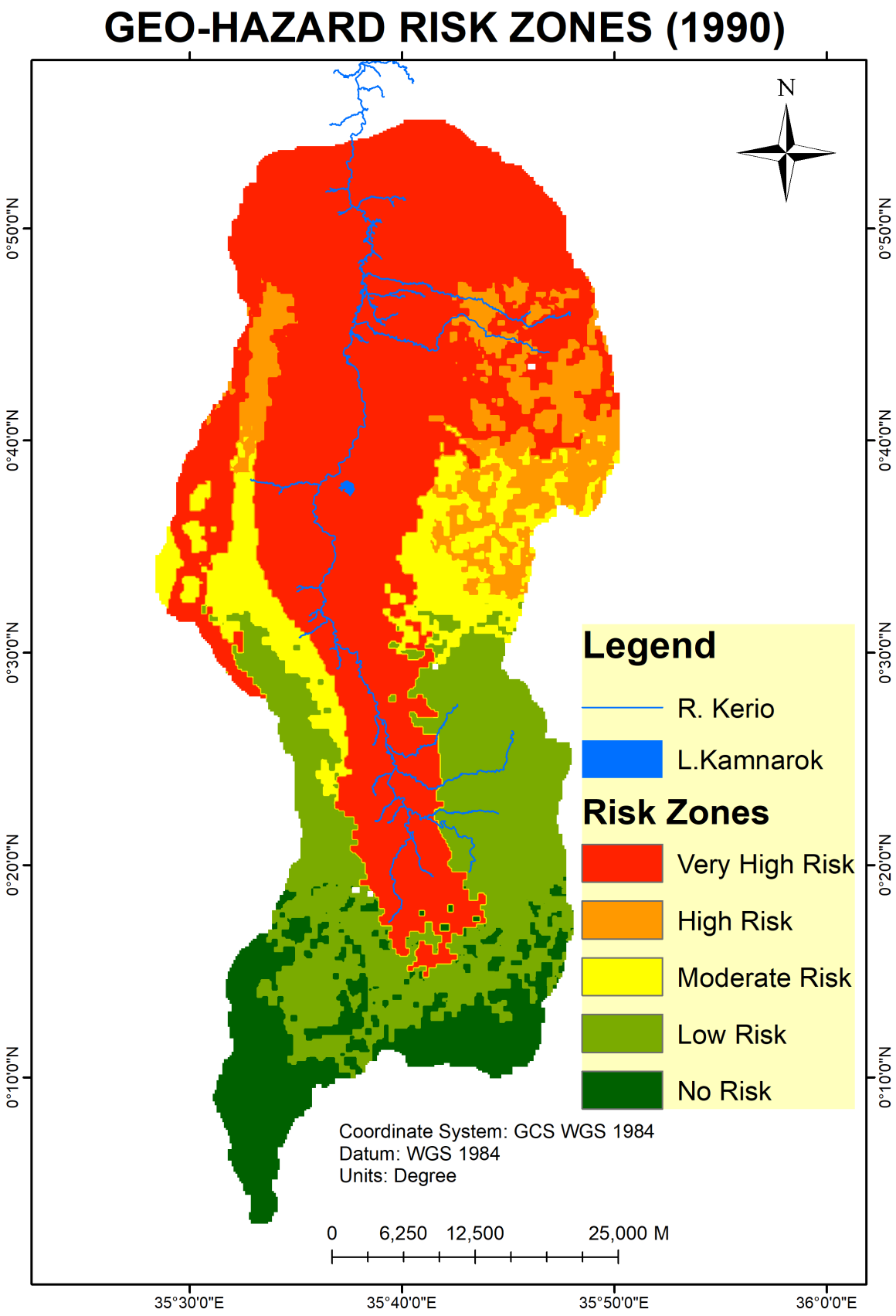
GEO-HAZARD RISK ZONES (1990)
N
0°50'0"N
0°40'0"N
0°30'0"N
0°20'0"N
0°10'0"N
35°30'0"E
35°40'0"E
35°50'0"E
36°0'0"E
Legend
R. Kerio
L.Kamnarok
Risk Zones
Very High Risk
High Risk
Moderate Risk
Low Risk
No Risk
Coordinate System: GCS WGS 1984
Datum: WGS 1984
Units: Degree
0 6,250 12,500 25,000 M

(a)

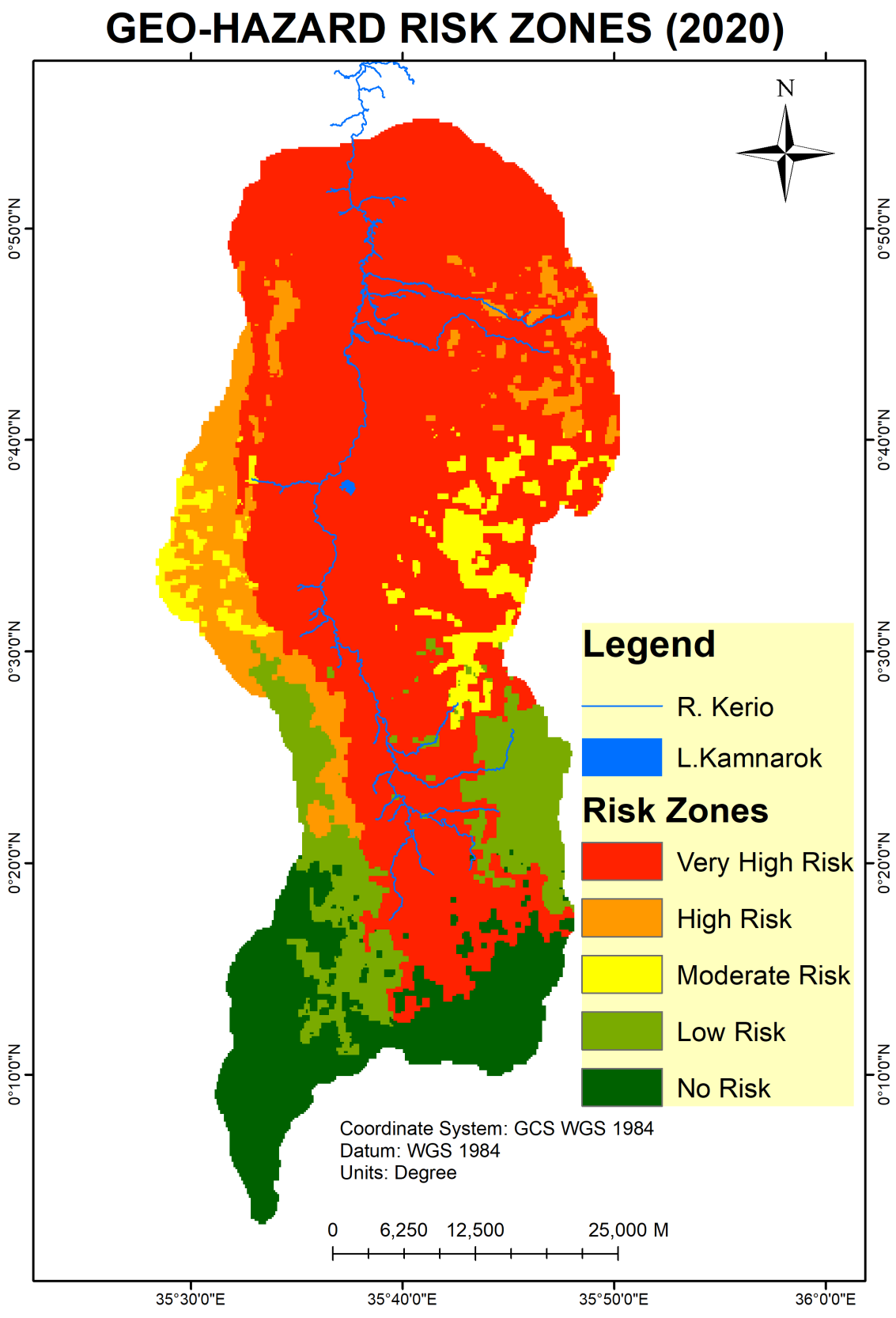

(b)

Figure 17. (a) 1990 geohazard risk zones, (b) 2020 geohazard risk zones.

4. Conclusions and Recommendations

From the land use, land cover maps, it was concluded that over the years deforestation has been a major occurrence in the basin where the area coverage of forests reduced by approximately 8.25% which equates to 22,209.59 ha loss of forest area. Therefore, setting up forest conservation programs such as afforestation should be encouraged by the local communities and governments to curb this menace. Forest conservation practices such as afforestation and reafforestation should be started and tree seedlings provided to all people living within the basin.

From the soil erosion maps it was concluded that annual soil loss increased in the basin massively from 1990 to 2020. Therefore, soil erosion control mechanisms should be encouraged to the local communities in the basin. These methods among others include: planting of trees, contour and across slope farming and strip cropping.

By 2020 approximately 75.65% of the total area of the basin had been classified as a moderate to very high-risk zone which meant that majority of the basin was susceptible to hazards such as soil erosion and mudslides. Therefore, it is recommended that preventive measures, early warning systems and evacuation procedures should be established by the local administrative governments. Such hazards pose risk to the communities living around the basin area hence impacting negatively on their livelihoods.

Acknowledgements

We acknowledge support from Dedan Kimathi University of Technology and Mapinfotek Geomatiks Ltd for the provision of time and support to work on research and development.

Authors' Contributions

Conceptualization, M. B.; methodology, J. G.; software, J. G.; validation, M. B.; formal analysis, J. G.; investigation, J. G.; resources, J. G; data curation, J. G.; writing—original draft preparation, J. G.; writing—review and editing, J. G; visualization, J. G.; supervision, M. B.; project administration, M. B.; funding acquisition, M. B. All authors have read and agreed to the published version of the manuscript.

Funding

This research received no external funding.

Data Availability Statement

All data and resources are available in the text or sources cited in the text.

Conflicts of Interest

The authors declare no conflict of interest.

References

[1] LEARNZ (2021) What Are Geohazards? https://www.learnz.org.nz/geohazards152/bg-standard-f/what-are-geohazards

[2] United States Department of Agriculture (2016) USLE History. https://www.ars.usda.gov/midwest-area/west-lafayette-in/national-soil-erosion-research/docs/usle-database/usle-history/#

[3] Sebastian, K. (2010) Agro-Ecological Zones of Africa. International Food Policy Research Institute, Washington DC. https://www.ifpri.org/publication/agro-ecological-zones-africa

[4] Balungi, F. (2010) Using GIS to Create an Agro-Climatic Zone Map for Soroti District. Geospatial World. https://www.geospatialworld.net/article/using-gis-to-create-an-agro-climatic-zone-map-for-soroti-district/

[5] Government of Canada (2015) Land Cover & Land Use. https://www.nrcan.gc.ca/maps-tools-and-publications/satellite-imagery-and-air-photos/tutorial-fundamentals-remote-sensing/educational-resources-applications/land-cover-biomass-mapping/land-cover-land-use/9373

[6] IPCC (2019) Climate Change and Land: an IPCC Special Report on Climate Change, Desertification, Land Degradation, Sustainable Land Management, Food Security, and Greenhouse Gas Fluxes in Terrestrial Ecosystems. In Press.

[7] Saina, C., Arusei, E., Kiptui, M. and Jemutai, J. (2016) The Causes and Socio Economic Impacts of Landslides in Kerio Valley, Kenya. *Merit Research Journals*, **4**, 58-66.

[8] Rijks, D.A., Woodhead, T. and Dagg, M. (1970) Evaporation in East Africa. *Bulletin of the International Association of Scientific Hydrology*, **15**, 61-67. https://doi.org/10.1080/02626667009493932

[9] Wischmeier, W.H. and Smith, D.D. (1978) Predicting Rainfall Erosion Losses—A Guide to Conservation Planning. Agriculture Handbook No. 537. US Department of Agriculture Science and Education Administration, Washington DC, 168 p.

[10] Boitt, M., Albright, O. and Kipkulei, H. (2020) Assessment of Soil Erosion and Climate Variability on Kerio Valley Basin, Kenya. *Journal of Geoscience and Environment Protection*, **8**, 97-114. https://doi.org/10.4236/gep.2020.86008

[11] Jiang, B.Y., Bamutaze, Y. and Pilesjö, P. (2014) Climate Change and Land Degradation in Africa: A Case Study in the Mount Elgon Region, Uganda. *Geo-Spatial Information Science*, **17**, 39-53. https://doi.org/10.1080/10095020.2014.889271

[12] Kassam, A.H., Velthuizen, H.T., Mitchell, A.J.B., Fischer, G.W. and Shah, M.M. (1992) Agro-Ecological Land Resources Assessment for Agricultural Development Planning: A Case Study of Kenya: Resources Data Base and Land Productivity. FAO, Rome. http://www.fao.org

[13] Stone, R.P. and Hilborn, D. (2012) Universal Soil Loss Equation (USLE) Factsheet. Ministry of Agriculture, Food and Rural Affairs, Ontario.

[14] Kouli, M., Soupios, P. and Vallianatos, F. (2009) Soil Erosion Prediction Using the Revised Universal Soil Loss Equation (RUSLE) in a GIS Framework, Chania, Northwestern Crete, Greece. *Environmental Geology*, **57**, 483-497. https://doi.org/10.1007/s00254-008-1318-9

[15] Durigon, V.L., Carvalho, D.F., Antunes, M.A.H., Oliveira, P.T.S. and Fernandes, M.M. (2014) NDVI Time Series for Monitoring RUSLE Cover Management Factor in a Tropical Watershed. *International Journal of Remote Sensing*, **35**, 441-453. https://doi.org/10.1080/01431161.2013.871081

[16] Colman, C.B. (2018) Impacts of Climate and Land Use Changes on Soil Erosion in the Upper Paraguay Basin. Federal University of Mato Grosso do Sul, Campo Grande.

[17] Congedo, L. (2021) Semi-Automatic Classification Plugin: A Python Tool for the Download and Processing of Remote Sensing Images in QGIS. *Journal of Open Source Software*, **6**, Article No. 3172.

[18] Liu, D.J., Run-Jie, L.I., Wang, W.Q. and Wei, G.J. (2006) Completion of Xining City Soil Erosion Monitoring Based on GIS. *Research of Soil and Water Conservation*, **13**, 111-114.

[19] Passage Technology (n.d.) What Is the Analytic Hierarchy Process (AHP)? https://www.passagetechnology.com/what-is-the-analytic-hierarchy-process

[20] Saaty, T.L. (1980) The Analytic Hierarchy Process. McGraw-Hill Book, Co., New York.

[21] Angelo, A.C.M. and Marujo, L.G. (2020) Life Cycle Sustainability Assessment and Decision-Making under Uncertainties. In: Ren, J.Z. and Toniolo, S., Eds., *Life Cycle Sustainability Assessment for Decision-Making*, Elsevier, Amsterdam, 253-268. https://doi.org/10.1016/B978-0-12-818355-7.00012-9

[22] Gompf, K., Traverso, M. and Hetterich, J. (2021) Using Analytical Hierarchy Process (AHP) to Introduce Weights to Social Life Cycle Assessment of Mobility Services. *Sustainability*, **13**, Article No. 1258. https://doi.org/10.3390/su13031258

[23] Jagoda, J., Schuldt, S. and Hoisington, A. (2020) What to Do? Let's Think It through! Using the Analytic Hierarchy Process to Make Decisions. *Frontiers for Young Minds*, **8**, Article No. 78. https://doi.org/10.3389/frym.2020.00078

[24] ArcGIS (2015) Analytic Hierarchy Process for ArcGIS. https://www.arcgis.com/home/item.html?id=bb3521d775c94b28b69a10cd184b7c1f

[25] FAO and UNEP (2020) The State of the World's Forests 2020: Forests, Biodiversity and People. FAO and UNEP, Rome. https://doi.org/10.4060/ca8642en

[26] Thebo, A.L., Drechsel, P. and Lambin, E.F. (2014) Global Assessment of Urban and Peri-Urban Agriculture: Irrigated and Rainfed Croplands. *Environmental Research Letters*, **9**, Article ID: 114002. https://doi.org/10.1088/1748-9326/9/11/114002

[27] d'Amour, C.B., Reitsma, F., Baiocchi, G., Barthel, S., Güneralp, B., Erb, K.H., Haberl, H., Creutzig, F. and Seto, K.C. (2017) Future Urban Expansion and Global Croplands. *Proceedings of the National Academy of Sciences of the United States of America*, **114**, 8939-8944. https://doi.org/10.1073/pnas.1606036114

[28] Study.com (2013) Problems in Agriculture: Loss of Land and Decreased Varieties. https://study.com/academy/lesson/problems-in-agriculture-loss-of-land-decreased-varieties-smaller-crop-yields.html

[29] Boitt, M., Mundia, C. and Pellikka, P. (2014) Modelling the Impacts of Climate Change on Agro-Ecological Zones—A Case Study of Taita Hills, Kenya. *Geosciences Journal*, **2**, 172-179.